

1 **The effect of molnupiravir and nirmatrelvir on SARS-CoV-2**
2 **genome diversity in severe models of COVID-19.**

3

4 Rebekah Penrice-Randal^{1*†}, Eleanor G. Bentley^{1*}, Parul Sharma¹, Adam Kirby¹, I'ah
5 Donovan-Banfield^{1,2}, Anja Kipar^{1,3}, Daniele F. Mega¹ Chloe Bramwell^{1,4}, Joanne
6 Sharp^{4,5}, Andrew Owen^{4,5}, Julian A. Hiscox^{1,2,6} and James P. Stewart^{1,5}.

7

8 ¹Department of Infection Biology and Microbiomes, University of Liverpool, Liverpool,
9 UK.

10 ²NIHR Health Protection Research Unit in Emerging and Zoonotic Infections,
11 Liverpool, UK.

12 ³Laboratory for Animal Model Pathology, Institute of Veterinary Pathology, Vetsuisse
13 Faculty, University of Zurich, Switzerland.

14 ⁴Department of Pharmacology and Therapeutics, University of Liverpool, UK.

15 ⁵Centre of Excellence in Long-acting Therapeutics (CELT), University of Liverpool,
16 UK.

17 ⁶A*STAR Infectious Diseases Laboratories (A*STAR ID Labs), Agency for Science,
18 Technology and Research (A*STAR), Singapore.

19

20 *These authors contributed equally.

21 † Corresponding author: rebee@liverpool.ac.uk

22

23 **Running title:** Antiviral and SARS-CoV-2 genome diversity

24

25 **Synopsis**

26 **Objectives.** Immunocompromised individuals are susceptible to severe COVID-19
27 and potentially contribute to the emergence of variants with altered pathogenicity due
28 to persistent infection. This study investigated the impact of immunosuppression on
29 SARS-CoV-2 infection in k18-hACE2 mice and the effectiveness of antiviral
30 treatments in this context during the first 7 days of infection.

31 **Methods** Mice were immunosuppressed using cyclophosphamide and infected with
32 a B daughter lineage of SARS-CoV-2. Molnupiravir and nirmatrelvir, alone and in
33 combination, were administered and viral load and viral sequence diversity was
34 assessed.

35 **Results** Treatment of infected but immune compromised mice with both compounds
36 either singly or in combination resulted in decreased viral loads and pathological
37 changes compared to untreated animals. Treatment also abrogated infection of
38 neuronal tissue. However, no consistent changes in the viral consensus sequence
39 were observed, except for the emergence of the S:H655Y mutation. Molnupiravir, but
40 not nirmatrelvir or immunosuppression alone, increased the transition/transversion
41 (Ts/Tv) ratio, representative of G>A and C>U mutations and this increase was not
42 altered by the co-administration of nirmatrelvir with molnupiravir.

43 Notably, immunosuppression itself did not appear to promote the emergence of
44 mutational characteristic of variants of concern (VOCs).

45 **Conclusions** Further investigations are warranted to fully understand the role of
46 immunocompromised individuals in VOC development, especially by taking
47 persistence into consideration, and to inform optimised public health strategies. It is
48 more likely that immunodeficiency promotes viral persistence but does not
49 necessarily lead to substantial consensus-level changes in the absence of antiviral
50 selection pressure. Consistent with mechanisms of action, molnupiravir showed a
51 stronger mutagenic effect than nirmatrelvir in this model.

52 **Keywords**

53 SARS-CoV-2, COVID-19, immunocompromised, intra-host evolution, Molnupiravir,
54 Nirmatrelvir, Paxlovid.

55

56 **Introduction**

57

58 Unsurprisingly, since the start of the Severe Acute Respiratory Syndrome 2 (SARS-
59 CoV-2) pandemic and the first deposited genome sequences, and like other
60 coronaviruses, SARS-CoV-2 has diverged through single nucleotide polymorphism,
61 and homologous and heterologous recombination applications resulting in insertions
62 and deletions ^{1,2}. Over the course of the pandemic changes that have dominated
63 have resulted in increased transmissibility such as the P323L/D614G changes in
64 early 2020 ³⁻⁵, immune-evasion ⁶ and altered pathogenicity ⁷.

65

66 Founder effects, population bottlenecks, selection pressures and behaviour have
67 contributed to the diversification of the SARS-CoV-2 genome but also to the
68 apparent waves of different variants. Several Variants of Concern (VOCs) have
69 arisen that have a transmission advantage and/or potential immune evasion. Some
70 reports have suggested that such variants may have arisen in hosts with
71 compromised immunity and/or persistent infections, where infection leads to the
72 generation of more diverse variants through longer viral evolution within an individual
73 ⁸. This includes a changing landscape of dominant viral genome sequence and
74 minor genomic variants in immune compromised individuals e.g. in a patient with
75 cancer ⁹. Changes within the individual mapped to several different regions on the
76 SARS-CoV-2 genome including the spike glycoprotein and orf8.

77

78 Complicating the picture of potential rapid and dramatic genomic change in immune
79 compromised hosts is that similar changes can be observed in immune competent
80 patients. This can be either as part of the dominant genomic sequence ¹⁰ or minor
81 variant genomes ¹. Indeed, genomic variants with deletions can be identified in the
82 minor genomic variant population of Middle East respiratory syndrome coronavirus
83 (MERS-CoV) from patients ¹¹ and as part of the dominant genomic sequence in
84 camels ^{12,13}.

85

86 Parallels with other animal coronaviruses can be found where persistent infections
87 are established, and this might be associated in pathogenicity; an example are feline
88 coronavirus (FCoV) infections and feline infectious peritonitis (FIP)¹⁴⁻¹⁷. Thus, one
89 concern with long term persistence of SARS-CoV-2 in immune compromised
90 patients is that new transmissible variants could emerge⁸.

91

92 Three small molecule direct acting anti-virals (DAAs) have received early use
93 authorisation for the treatment of COVID-19: remdesivir, molnupiravir (both
94 nucleoside analogues which target viral nucleic acid synthesis) and nirmatrelvir
95 (which targets the main viral protease). Unlike remdesivir, molnupiravir and
96 nirmatrelvir are orally administered and thus more readily deployed for treatment in
97 the community. Nirmatrelvir is packaged with ritonavir (as Paxlovid), this later
98 molecule acting as a pharmacokinetic boosting agent to inhibit P450 (CYP) 3A4.
99 However, adequate nirmatrelvir plasma concentrations can be achieved in mice
100 without the need for ritonavir boosting. In cell culture single or combination treatment
101 can result in decreased viral replication^{18,19} and a natural extension is that such anti-
102 virals may be deployed as combination therapy to reduce the emergence of resistant
103 genotypes²⁰. Resistant genotypes/phenotypes have been identified in vitro for
104 remdesivir²¹. Molnupiravir has previously been shown to enhance viral
105 transition/transversion mutations in a phase II clinical trial²² and a molnupiravir
106 associated signature has been identified in circulating SARS-CoV-2 lineages since
107 the introduction of molnupiravir in 2022²³.

108

109 Immunocompromised patients with a SARS-CoV-2 infection are treated as a priority
110 with anti-virals, including those compounds that generically target virus replication by
111 causing hyper-mutation or specifically preventing the function of a viral protein critical
112 to the life cycle of the virus. Such anti-virals may be deployed as combination
113 therapy to reduce the emergence of resistant genotypes²⁰ and may be particularly
114 relevant for patients with compromised immunity²⁴. However, in the latter patients,
115 anti-virals may decrease viral loads but enhance genomic plasticity. To investigate
116 this, the genomic variation of SARS-CoV-2 was evaluated in an immune
117 compromised host over the first 7 days of infection, in the absence and presence of
118 medical countermeasures. We have developed animal models of COVID-19 to be
119 able to assess pathogenicity of new variants and develop interventions²⁵⁻²⁷. An

120 immune suppressed K18-hACE2 transgenic mouse model was used to simulate
121 patients with severe COVID-19^{28,29}. Two anti-virals, molnupiravir and nirmatrelvir,
122 were evaluated either singly or in combination.

123 **Methods**

124

125 **Animal infection and treatment**

126 A UK variant of SARS-CoV-2 (hCoV-2/human/Liverpool/REMRQ0001/2020), was
127 used as described previously^{30,31}. Mutations belonging to the B daughter lineage
128 virus are outlined in table 1.

129

130 **Table 1: Input virus used in this study**

131

| Input virus | | |
|--------------------------|-------------|--------------------------|
| Nucleotide change | Gene | Amino Acid Change |
| A6948C | Nsp3 | N1410T or N2228T |
| G11083T | Nsp6 | L37F or L3606F |
| C21005T | Nsp16 | A116V or A2513V |
| C25452T | Orf3a | I20 no change |
| C28253T | Orf8 | F120 no change |

132

133

134 Animal work was approved by the local University of Liverpool Animal Welfare and
135 Ethical Review Body and performed under UK Home Office Project Licence
136 PP4715265. Transgenic mice carrying the human ACE2 gene under the control of
137 the keratin 18 promoter (K18-hACE2; formally B6.Cg-Tg(K18-ACE2)2PrImn/J) were
138 purchased from Jackson Laboratories (France) at 8 – 10 weeks of age. Mice were
139 maintained under SPF barrier conditions in individually ventilated cages and
140 underwent a week of acclimatisation in these conditions prior to experimental use.

141

142 Experimental design is shown in Fig. 1 and treatment groups detailed in Table 2.
143 Animals were randomly assigned into multiple cohorts of four animals using a
144 random number generator. For operational reasons at high containment the
145 treatment groups were not blinded during the experiment. Sample size was
146 determined using prior experience of similar experiments with SARS-CoV-2. For
147 SARS-CoV-2 infection, mice were anaesthetized lightly with isoflurane and
148 inoculated intra-nasally with 50 µl containing 10⁴ PFU SARS-CoV-2 in PBS as
149 described previously²⁶. Some cohorts of mice were immunosuppressed by
150 treatment with cyclophosphamide (100 mg/kg) intra-peritoneally (IP) at day -4 and -1
151 pre-infection. Molnupiravir was made up in 10% PEG400 and 2.5% cremophor in

152 water and used at 100 mg/kg. Nirmatrelvir was dissolved in 2% Tween 80 in 98%
153 (v/v) of 0.5% methyl cellulose and used at 500 mg/kg. These does were chosen
154 based on the known therapeutic range for these drugs in mice ³²⁻³⁵. Both drugs were
155 administered via the oral route one hour prior to infection and then twice daily up to 4
156 days post-infection via the oral (PO) route. Groups of animals were kept in the same
157 cages during the experiment and were always weighed and treated in the same
158 order. Mice were sacrificed at day 6 (vehicle and cyclophosphamide treated group)
159 or 7 (all others) after infection by an overdose of pentobarbitone. Weights were
160 recorded daily, and tissues were removed immediately for downstream processing.
161 The right lung and nasal turbinates were frozen at -80 °C until further processing.
162 The left lung and heads were fixed in 10% neutral buffered formalin for 24-48 h and
163 then stored in 70%. No data were excluded from the analyses.

164

165 **Histology, immunohistology and morphometric analysis**

166 The fixed left lung was routinely paraffin wax embedded. Heads were sawn
167 longitudinally in the midline using a diamond saw (Exakt 300; Exakt) and the brain
168 left in the skull. Heads were gently decalcified in RDF (Biosystems) for twice 5 days,
169 at room temperature and on a shaker, then both halves paraffin wax embedded.
170 Consecutive sections (3-5 µm) were either stained with hematoxylin and eosin (HE)
171 or used for immunohistology (IH). IH was performed to detect viral antigen
172 expression using the horseradish peroxidase method and a rabbit anti-SARS-CoV
173 nucleocapsid protein (Rockland, 200-402-A50) as primary antibody, as previously
174 described ^{26,36,37}.

175 For morphometric analysis, the immunostained sections were scanned
176 (NanoZoomer-XR C12000; Hamamatsu, Hamamatsu City, Japan) and analysed
177 using the software program Visiopharm (Visiopharm 2020.08.1.8403; Visiopharm,
178 Hoersholm, Denmark) to quantify the area of viral antigen expression in relation to
179 the total area (area occupied by lung parenchyma) in the sections. This was used to
180 compare the extent of viral antigen expression in the lungs between the different
181 treatment groups. A first app was applied that outlined the entire lung tissue as ROI
182 (total area). For this a Decision Forest method was used and the software was
183 trained to detect the lung tissue section (total area). Once the lung section was
184 outlined as ROI the lumen of large bronchi and vessels was manually excluded from

185 the ROI. Subsequently, a second app with Decision Forest method was trained to
186 detect viral antigen expression (as brown DAB precipitate) within the ROI.

187

188 **RNA extraction**

189 To inactivate virus in throat swabs, 260 μ L of swab buffer was inactivated in a Class
190 II Biosafety cabinet using 750 μ L of TRIzol LS reagent (ThermoFisher, Runcorn,
191 UK), and transferred into 2 mL screw-cap vials and mixed. Samples were stored at
192 -80°C until further analysis. RNA samples were normalised to 20ng/ μ l before qPCR
193 and sequencing.

194

195 **qRT-PCR for viral load**

196 Viral loads were quantified using the GoTaq[®] Probe 1-Step RT-qPCR System
197 (Promega). For quantification of SARS-CoV-2 the nCOV_N1 primer/probe mix from
198 the SARS-CoV-2 (2019-nCoV) CDC qPCR Probe Assay (IDT) were utilised and
199 murine 18S primers as described previously^{25,26}.

200

201 **Sequencing of SARS-CoV-2**

202 RNA samples were placed into plates based on very high viral load (Ct<18), high
203 viral load (Ct 20-24), medium viral load (Ct 25-28) or low viral load (Ct >28) to assist
204 with pooling strategy. Library preparation consisted of converting RNA to cDNA
205 using LunaScriptTM (Thermofisher), then amplified by reverse complement (RC)-PCR
206 amplification (EasySeqTM SARS-CoV-2 Whole Genome Sequencing kit, Nimagen,
207 Netherlands). This kit barcodes and ligates Illumina adapters in a single PCR
208 reaction, with two separate pools of primers (pools 1 and 2). After amplification, each
209 amplicon library was pooled 1:1 before being cleaned with AmpliCleanTM beads and
210 quantification. The two pools were then added together and denatured 2 μ l, 4 μ l, 8 μ l
211 and 16 μ l of each pool for very high, high, medium and low viral load was taken
212 respectively. Finally, the denatured amplicon library was loaded into the NovaSeq
213 cartridge (2 x 150 bp run).

214

215 **Bioinformatics**

216 Supplementary Fig. S1 provides an overview of the workflow used in this study. In
217 short, raw paired end fastq files were inputted into the EasySeq pipeline to generate
218 alignment files, vcf's and consensus sequences using the NC_045512.2 SARS-CoV-

219 2 reference³⁸. Consensus sequences were inputted into Nextclade for lineage
220 assignment and bam files were inputted into DiversiTools
221 (<https://github.com/josephhughes/DiversiTools>) to assess global minor variation.
222 Sequencing data was analysed as previously described and statistical analysis and
223 visualisation was performed in R²². In brief, the entropy outputs from DiversiTools
224 was imported to R and a coverage of at least 100 at each position was required, the
225 average quality scores, derived from phred scoring, for each position was less than
226 2×10^{-6} indicative of low basecalling error. Raw fastq files are available under SRA
227 Project Accession: PRJNA886870. Code for analysis and figure generation is
228 available at <https://github.com/Hiscox-lab/viral-genomics-immunosuppression-and-countermeasures>.
229

230

231 **Statistics**

232 Graphs were prepared and statistics performed using Prism 10 (Graphpad Inc). *P*
233 values were set at 95% confidence interval. A repeated-measures two-way ANOVA
234 (Bonferroni post-test) was used for time-courses of weight loss; log-rank (Mantel-
235 Cox) test was used for survival curve and Mann-Whitney *U* test for side-by-side
236 comparisons. All differences not specifically stated to be significant were not
237 significant (*p* > 0.05). For all figures, **p* < 0.05.
238

239 **Results and Discussion**

240

241 Since the emergence of the Alpha VOC there has been discussion on the
242 involvement of the immunocompromised host and the generation of variants ^{8,39-43}.
243 There are many case studies in the literature that follow SARS-CoV-2 evolution in
244 immunocompromised hosts, however, the generation of VOCs is likely due to
245 persistent infection as opposed to immunocompromised immune systems itself, little
246 has been explored experimentally. In this study, mice were chemically
247 immunocompromised with cyclophosphamide which is known to efficiently remove
248 adaptive immunity in the form of B and T cells ⁴⁴. Additionally, therapeutic agents,
249 molnupiravir and nirmatrelvir, were used independently and in combination to
250 determine the effectiveness of these compounds in an immunocompromised model,
251 and the impact of these compounds on viral sequence diversity during the first 7
252 days of infection.

253

254 Modelling an immunocompromised state in animal models in the context of SARS-
255 CoV-2 is important for the consideration of countermeasures that may be utilised for
256 humans who are considered vulnerable. Cyclophosphamide has been used
257 previously to study the impact of immunosuppression in a hamster model ⁴⁵⁻⁴⁷, where
258 intranasally infected hamsters with cyclophosphamide treatment before infection had
259 prolonged weight loss and an inadequate neutralising antibody response to SARS-
260 CoV-2. Distinct transcriptional profiles were identified between immunocompetent
261 and immunosuppressed animals; however, the impact of antivirals or viral genome
262 diversity was not investigated.

263

264 To investigate the frequency of genomic changes that occur in SARS-CoV-2 in the
265 immune compromised or competent host in the presence or absence of antiviral
266 drugs, K18-hACE2 transgenic mice were used as a model for severe SARS-CoV-2
267 infection in humans ⁴⁸. We have found that the pathological changes in the lungs in
268 this model in many aspects resemble those in humans who have died of severe
269 COVID-19 ^{26,28,29,36,37}. To mimic a host with compromised immunity, an experimental
270 protocol was developed in which mice were exposed to cyclophosphamide ⁴⁴ (Fig. 1,
271 Table 2). Several anti-viral regimes in humans were simulated in the mouse model
272 by giving a human equivalent dose of either molnupiravir (100 mg/kg), nirmatrelvir

273 (500 mg/kg) or both in combination. This included prophylactic followed by
274 therapeutic treatment. Mice were infected with 10^4 PFU of SARS-CoV-2.

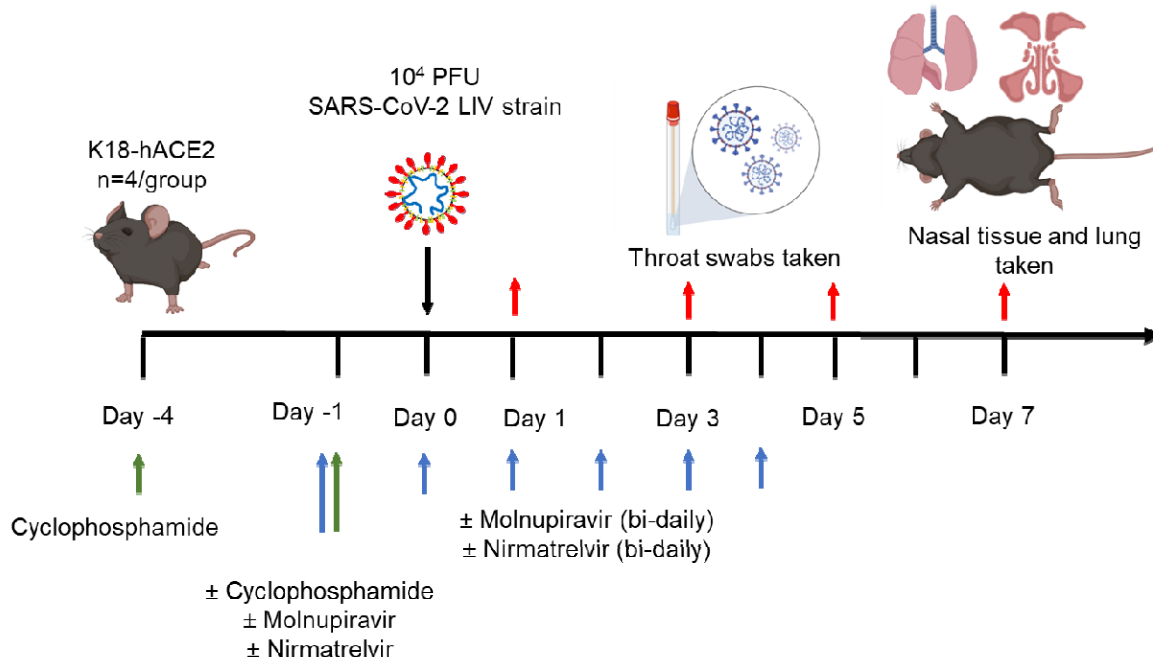


Figure 1. Schematic diagram of the experimental design for infection of immune compromised K18-hACE2 mice with SARS-CoV-2 and evaluation of two antiviral drugs given at a human equivalent dose; molnupiravir, a broad acting compound causing error catastrophe, or nirmatrelvir which specifically targets the viral 3C-like protease. Cyclophosphamide was used at 100 mg/kg via the intraperitoneal route to immunosuppress mice. Molnupiravir was used at 100 mg/kg and nirmatrelvir at 500 mg/kg both via the oral route. Effects of infection and treatment were evaluated by measuring the weight of the mice daily, determining viral loads in sequential oral/throat swabs and at day 7 post infection, and examining nose, brain and lung at day 7 post infection for any histological changes and the expression of SARS-CoV-2 nucleoprotein.

275

276 **Table 2. Treatment groups for in vivo analysis**

| Group | Treatment |
|-------|------------------------------------------------|
| 1 | Control (vehicle) |
| 2 | Cyclophosphamide |
| 3 | Molnupiravir |
| 4 | Cyclophosphamide + molnupiravir |
| 5 | Cyclophosphamide + nirmatrelvir |
| 6 | Cyclophosphamide + molnupiravir + nirmatrelvir |

277

278

279 **Treatment with Molnupiravir or Nirmatrelvir either individually or in**
280 **combination provides recovery in immune compromised mice infected with**
281 **SARS-CoV-2.**

282 Cyclophosphamide treatment prior to SARS-CoV-2 infection of hACE2 mice led to a
283 more pronounced early weight loss in comparison to immunocompetent mice, a
284 phenomenon previously reported in hamsters ⁴⁷. This was not associated with earlier
285 mortality than in vehicle treated immunocompetent mice, although in human, a
286 delayed adaptive immune response has been shown to be associated with fatality in
287 COVID-19 patients, which may have been observed over longer timeframes ⁴⁹. Daily
288 weighing of the animals indicated that all groups lost body weight after day 1 (Fig. 2).
289 We attribute this to aversion to eating as all therapies were applied by gavage.
290 However, starting at day 3 all groups, except for mice exposed to cyclophosphamide,
291 or mice exposed to cyclophosphamide and treated with molnupiravir, started to gain,
292 or stabilise weight. By days 5 and 6 a clear pattern had emerged where all groups
293 treated with molnupiravir or nirmatrelvir either individually or in combination had
294 regained their starting weight. The exception to this were mice exposed to vehicle
295 only (controls) or cyclophosphamide; these reached a humane end point on day 6
296 (Fig. 2). Comparison of survival curves again indicated that immune compromised
297 animals treated either singly or in combination with each therapeutic went on to
298 survive (Fig. 3).

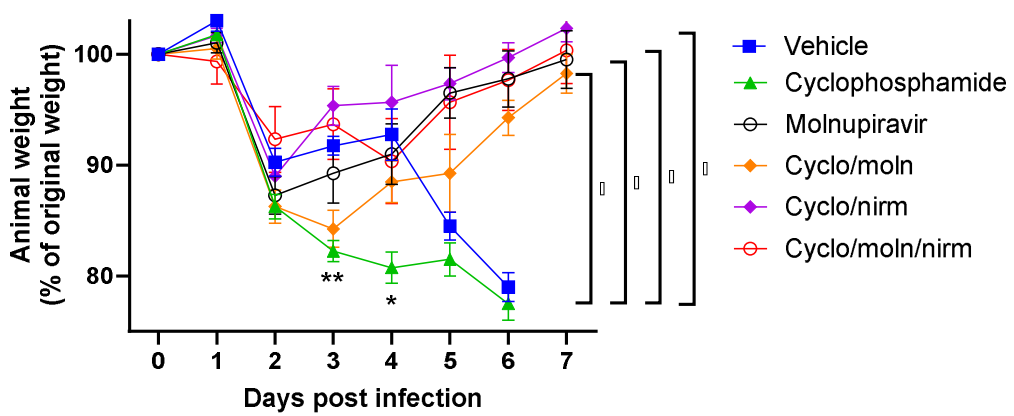
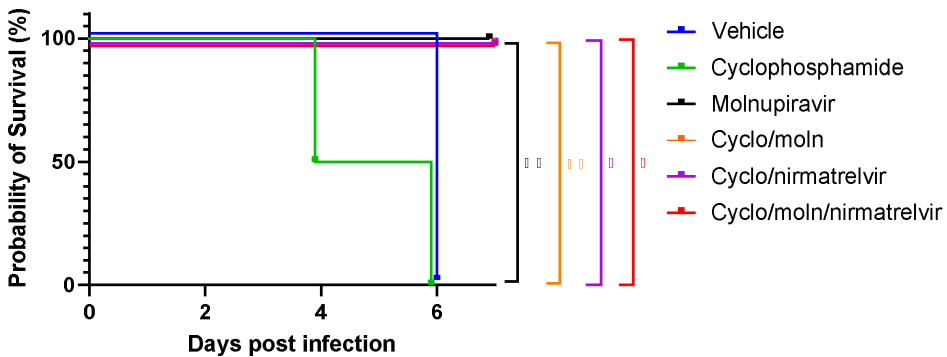


Figure 2: Treatment of SARS-CoV-2-infected mice leads to decreased weight loss. K18-hACE2 mice were challenged intranasally with 10^4 PFU SARS-CoV-2. Mice were monitored for weight at indicated time-points. (n = 4). Data represent the mean residual weight \pm SEM. Comparisons were made using a repeated-measures two-way ANOVA (Bonferroni post-test). * on the represents P < 0.05. Asterisks below the curves represent * P < 0.05 and ** P < 0.01 between the cyclophosphamide and vehicle groups. Brackets and asterisk at the side represents P < 0.05 for the Vehicle/cyclophosphamide groups and the drug treated groups.

299



300

301 **Figure 3: Treatment of SARS-CoV-2-infected mice leads to enhanced survival.**
302 *K18-hACE2 mice were challenged intranasally with 10⁴ PFU SARS-CoV-2. Survival*
303 *was assessed at indicated time points and significance determined using log rank*
304 *(Mantel-Cox) test (n = 4).*

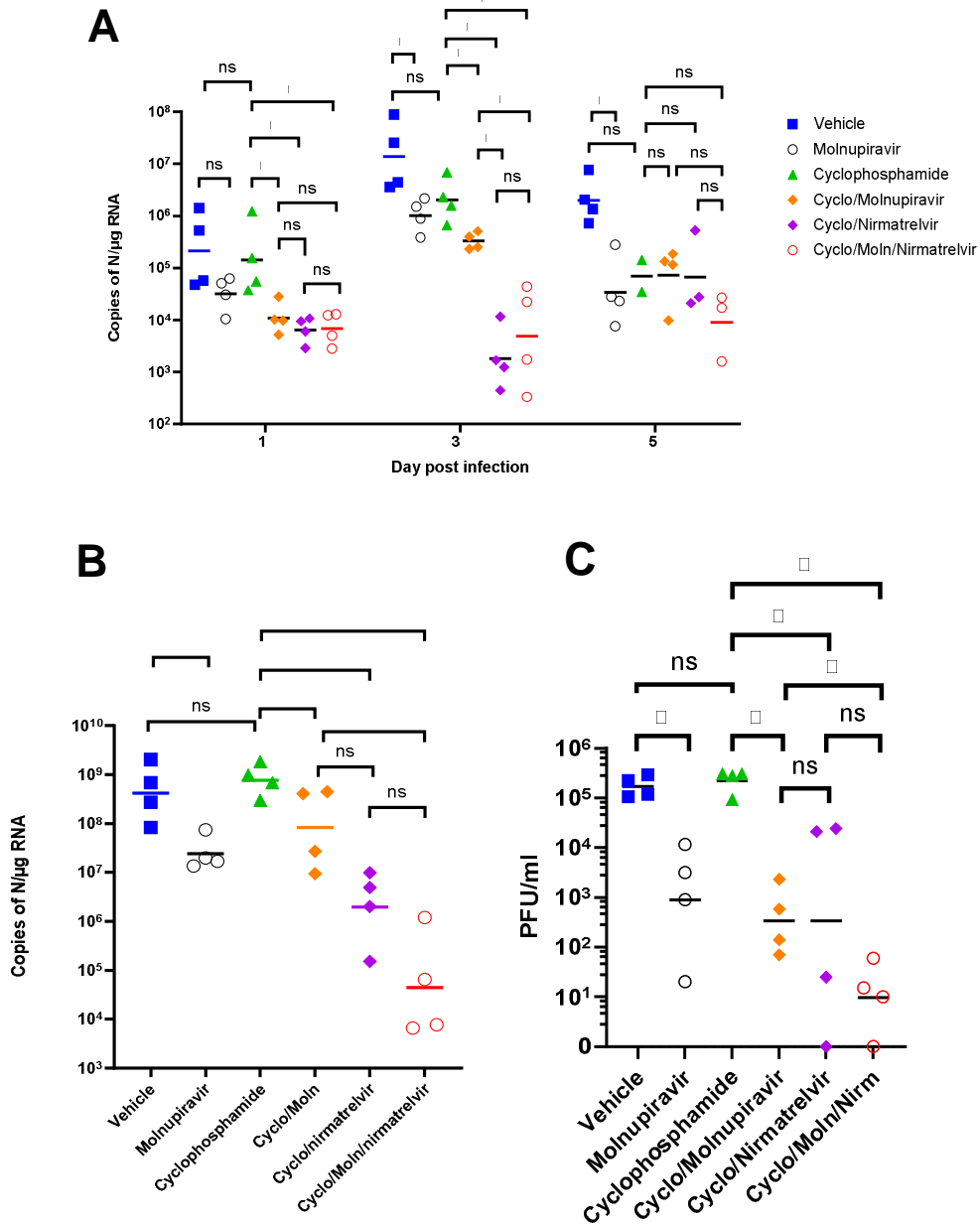
305

306 **Viral load decreases in immune compromised mice treated with Molnupiravir**
307 **or Nirmatrelvir either individually or in combination.**

308 Viral load in terms of copy numbers of the SARS-CoV-2 genome were calculated for
309 throat swabs during infection and compared to nasal tissue and lung tissue at the
310 end of the experiment. The data indicated that for throat swabs on days 1 and 3
311 post-infection there was a significant decrease in viral load in animals treated with
312 molnupiravir or nirmatrelvir either individually or in combination compared to
313 untreated controls (Figure 4A). At day 3 there was a significant difference between
314 both compounds used in combination and molnupiravir only (Figure 4A). No
315 significant differences were observed between vehicle control and
316 cyclophosphamide only groups.

317

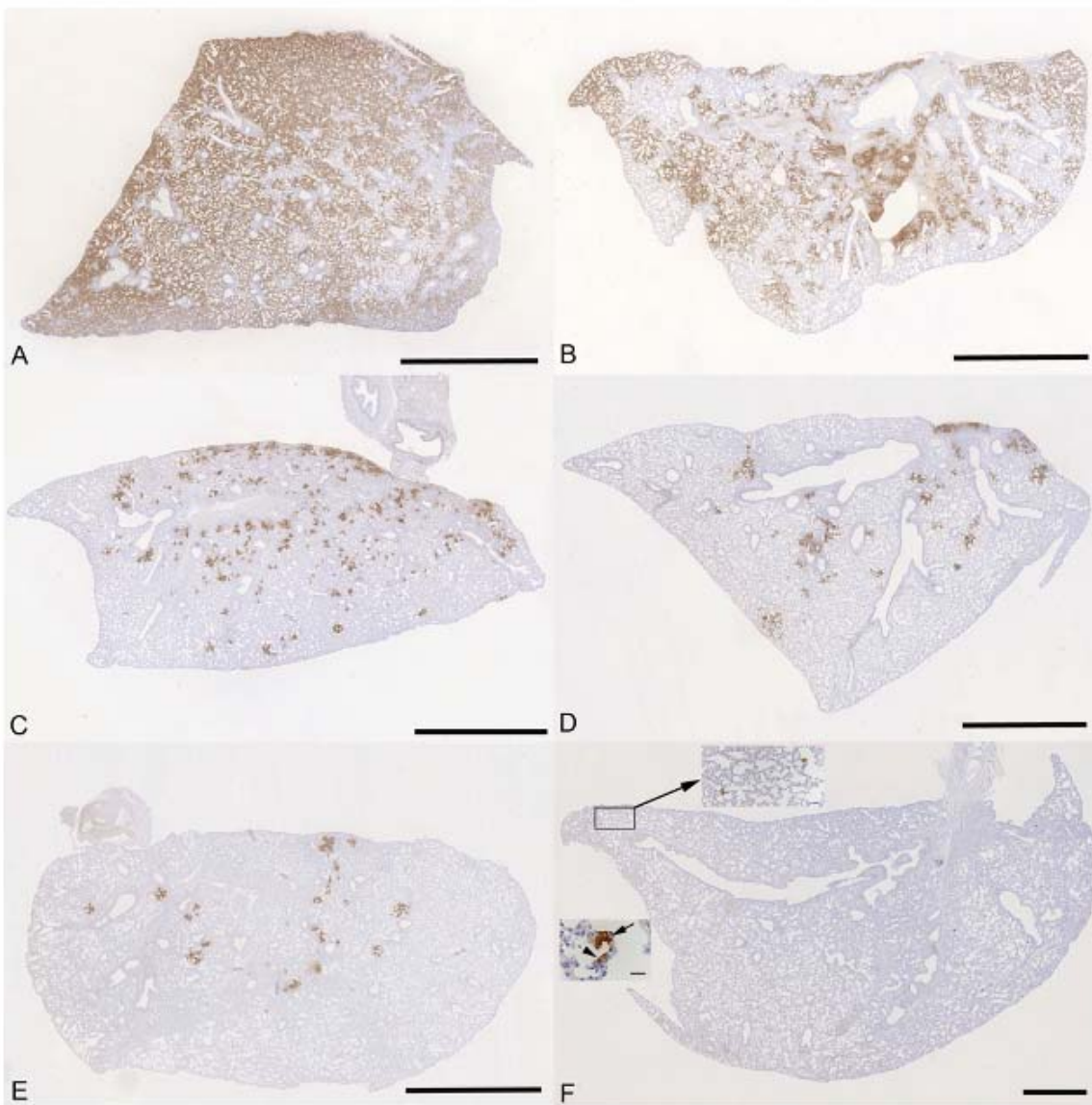
318 Comparison of viral loads and titres in nasal and lung tissue respectively (Figure 4B
319 and 4C, respectively) at day 7 post-infection reflected that there was a significantly
320 lower viral load in animals treated with molnupiravir or nirmatrelvir either individually
321 or in combination compared to untreated mice. However, nirmatrelvir treatment
322 resulted in a greater decrease in viral load compared to molnupiravir. The
323 molnupiravir/nirmatrelvir combination was also more effective at decreasing viral
324 load than either drug alone, but this was only statistically significant in the case of
325 molnupiravir vs the drug combination.



326

Figure 4. Viral loads in swabs and tissues. K18-hACE2 mice were challenged intranasally with 10^4 PFU SARS-CoV-2 and treated as indicated ($n = 4$ per group). RNA extracted from oral/throat swabs and nasal tissue was analysed for virus RNA load using qRT-PCR and primers specific for the SARS-CoV-2 N gene. Assays were normalised relative to levels of 18S RNA. Lung tissue was analysed for live virus by plaque assay. Data for individual animals are shown with the median value represented by a black line. (A) Throat swabs; (B) nasal tissue; (C) lung tissue. Comparisons were made using two-way ANOVA (Bonferroni post-test) in panel A and Mann-Whitney U test (Panels B and C). * Represents $p < 0.05$.

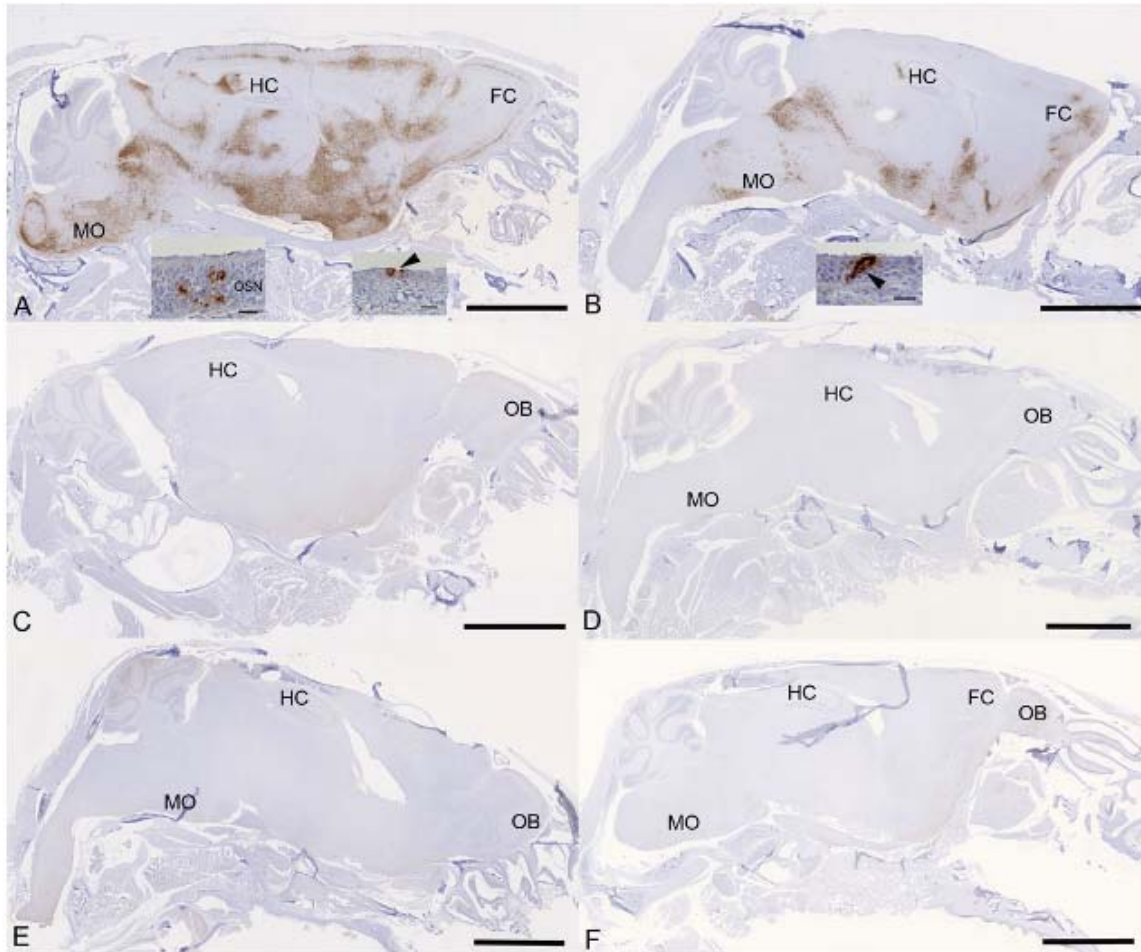
337 **Treatment with molnupiravir or nirmatrelvir or both in combination results in**
338 **marked reduction of pulmonary infection and inhibits viral spread to the brain.**
339 The lung, nose and brain of all animals were examined for any histopathological
340 changes and the expression of viral antigen by immunohistology, to determine
341 whether treatment of the animals with molnupiravir and/or nirmatrelvir influenced the
342 outcome of infection. The lungs of vehicle treated, immunocompetent animals
343 showed the typical changes previously reported in K18-hACE2 mice infected with
344 this virus strain ²⁶, i.e. multifocal areas with pneumocyte degeneration, type II
345 pneumocyte activation, mild neutrophil infiltration, and mild vasculitis, with a diffuse
346 increase in interstitial cellularity and widespread SARS-CoV-2 antigen expression in
347 alveolar epithelial cells (Fig. 5A). In mice that had received cyclophosphamide alone,
348 the changes were very similar, but slightly less widespread, with some unaltered
349 parenchyma and less extensive viral antigen expression (Fig. 5B). With molnupiravir
350 treatment, both inflammatory processes and viral antigen expression were markedly
351 decreased; indeed, SARS-CoV-2 antigen was only found in disseminated patches of
352 alveoli with positive pneumocytes (Fig. 5C). With cyclophosphamide and
353 molnupiravir treatment, the lung parenchyma was widely unaltered, and there were
354 only small patches of inflammation and alveoli with viral antigen expression,
355 respectively (Fig. 5D). These were further reduced in number and size in animals
356 that had received cyclophosphamide and nirmatrelvir (Fig. 5E). Treatment with all
357 three compounds, cyclophosphamide, molnupiravir and nirmatrelvir, resulted in
358 widely unaltered lung parenchyma with no or minimal viral antigen expression (Fig.
359 5F).



360

361 **Figure 5:** K18-hACE2 mice were challenged intranasally with 10^4 PFU SARS-CoV-2 and
362 treated as indicated below ($n = 4$ per group). Immunohistology for the detection of viral
363 antigen in the lung at day 6 or 7 post infection. Sections from the formalin-fixed, paraffin
364 embedded left lung lobe were stained using anti-SARS-CoV nucleoprotein and
365 counterstained with hematoxylin. Representative images from the individual treatment
366 groups are shown as follows: A. vehicle; B. cyclophosphamide; C. molnupiravir; D.
367 cyclophosphamide and molnupiravir; E. cyclophosphamide and nirmatrelvir; F.
368 cyclophosphamide, molnupiravir and nirmatrelvir. Viral antigen expression is restricted to
369 pneumocytes in a few individual alveoli (higher magnifications in insets). Bars represent 2.5
370 mm (A-E), 1 mm (F) and 20 μ m (F, insets).

371 Examination of the heads using longitudinal sections (midline) revealed consistent
372 and widespread infection of the brain in animals treated with the vehicle or with
373 cyclophosphamide alone (Fig. 6A, B); this was associated with mild perivascular
374 mononuclear infiltration in particular in the brain stem, as described before in K18-
375 hACE2 mice infected with this virus strain ³⁷. In both groups of animals,
376 immunohistology confirmed viral antigen expression in the respiratory and/or
377 olfactory epithelium, in the latter with evidence of infection in olfactory sensory
378 neurons (Fig. 6A, B). In the other groups, there was no evidence of viral infection of
379 the brain (Fig. 6C-F), and viral antigen expression in the nasal mucosa was not seen
380 or restricted to scattered individual epithelial cells. In vehicle control and
381 cyclophosphamide mice, the nasal mucosa harboured viral antigen at this stage, in
382 the respiratory epithelium and in the olfactory epithelium; in the latter it also
383 appeared to be present in sensory neurons. Consequently, the virus had reached
384 and spread widely in the brain where it was detected in neurons; the infection was
385 associated with mild inflammatory response in particular in the brain stem, as
386 described before in K18-hACE2 mice infected with this virus strain ^{26,37}. After
387 treatment with all three compounds, cyclophosphamide, molnupiravir and
388 nirmatrelvir, the lung parenchyma was basically unaltered, with no or minimal viral
389 antigen expression. In all groups of mice, viral antigen expression in the nasal
390 mucosa was not seen or restricted to scattered individual epithelial cells and there
391 was no evidence of viral infection of the brain, suggesting that the antiviral treatment
392 blocked infection of the brain. Whether the latter is purely a consequence of reduced
393 viral replication in the upper respiratory tract cannot be assessed in the present
394 study; it does, however, appear likely.



395

396 **Figure 6:** K18-hACE2 mice were challenged intranasally with 10^4 PFU SARS-CoV-2 and
397 treated as indicated below ($n = 4$ per group). Immunohistology for the detection of viral
398 antigen in the brain and nose at day 6 or 7 post infection. Sections from formalin-fixed,
399 decalcified and paraffin embedded heads after longitudinal sawing in the midline were
400 stained using anti-SARS-CoV nucleoprotein, and counterstained with hematoxylin. Only
401 small fragments of nasal mucosa were available for the examination, as the nasal turbinates
402 had been sampled for PCR. Representative images from the individual treatment groups are
403 shown as follows: **A.** Vehicle. There is widespread infection of the brain. The insets show
404 infection of individual cells with the morphology of olfactory sensory neurons and epithelial
405 cells in the olfactory epithelial layer (left inset) and individual respiratory epithelial cells in the
406 nasal mucosa (arrowhead; right inset); **B.** Cyclophosphamide. There is widespread infection
407 of the brain. The inset shows a group of positive epithelial cells/sensory neurons in the
408 olfactory epithelial layer (arrowhead); **C.** Molnupiravir. There is no evidence of brain
409 infection. **D.** Cyclophosphamide and molnupiravir. There is no evidence of brain infection. **E.**
410 Cyclophosphamide and nirmatrelvir. There is no evidence of brain infection. **F.** Cyclophosphamide,
411 molnupiravir and nirmatrelvir. There is no evidence of brain infection. Bars represent 2.5 mm (A-F) and 20 μ m (A, B insets). FC – frontal cortex, HC –
412 hippocampus, MO – medulla oblongata, OB – olfactory bulb, OSN - olfactory sensory
413 neurons.
414

415 **Evaluation of dominant and minor variants in SARS-CoV-2**

416 To determine the impact of immunosuppression on viral diversity, 116 RNA samples
417 from swabs and tissue were sequenced and analysed using the EasySeq WGS
418 protocol by Nimagen. alignment files and associated index files were inputted into
419 DiversiTools to provide mutation data and outputs were analysed in R. Samples with
420 less than 90% breadth of coverage were discarded for mutational analysis (n=12), as
421 well as samples that returned bad or mediocre quality scores in nextclade (n=13).
422 The samples that were excluded were associated with higher Ct values and later
423 time points belonging in the nirmatrelvir treatment groups. Sequencing data from 89
424 samples were taken forward in the analysis (swab, n=50, tissue n=39,
425 Supplementary Table S1).

426

427 The input virus contained 5 substitutions and 3 amino acid substitutions in
428 comparison to the reference sequence (NC_045512.2) and were thus not considered
429 as changes during the analysis (Table 1). The S: H655Y mutation was present in
430 76% of the genomes that passed QC at the dominant level and observed as a minor
431 variant across all samples (Supplementary Fig. S2). This mutation has been reported
432 previously as a spike adaptation to other species such as cats, hamsters, and mink
433 ⁵⁰⁻⁵² and of course has independently arisen in human lineages such as Omicron ⁵³.
434 As this mutation was clearly associated with a species adaptation, it was disregarded
435 for the evaluation of treatment and immune status driven mutations. The other
436 mutations appear to be novel at the time of writing; however, no distinct group was
437 associated with driving these mutations, and can be overall interpreted as a rare
438 event (Supplementary Table S2). The sequences showing the highest number of
439 mutations were sequences derived from tissue samples. The species-specific
440 adaptation S:H655Y was observed more frequently in the dataset, where there was
441 little evidence of adaptations specific to immunocompromised and antiviral
442 environments, putting the evolutionary pressures into perspective. Adaptations
443 associated with immunosuppression and antiviral treatment may emerge in the
444 context of persistent replication of the virus which would need to be investigated.

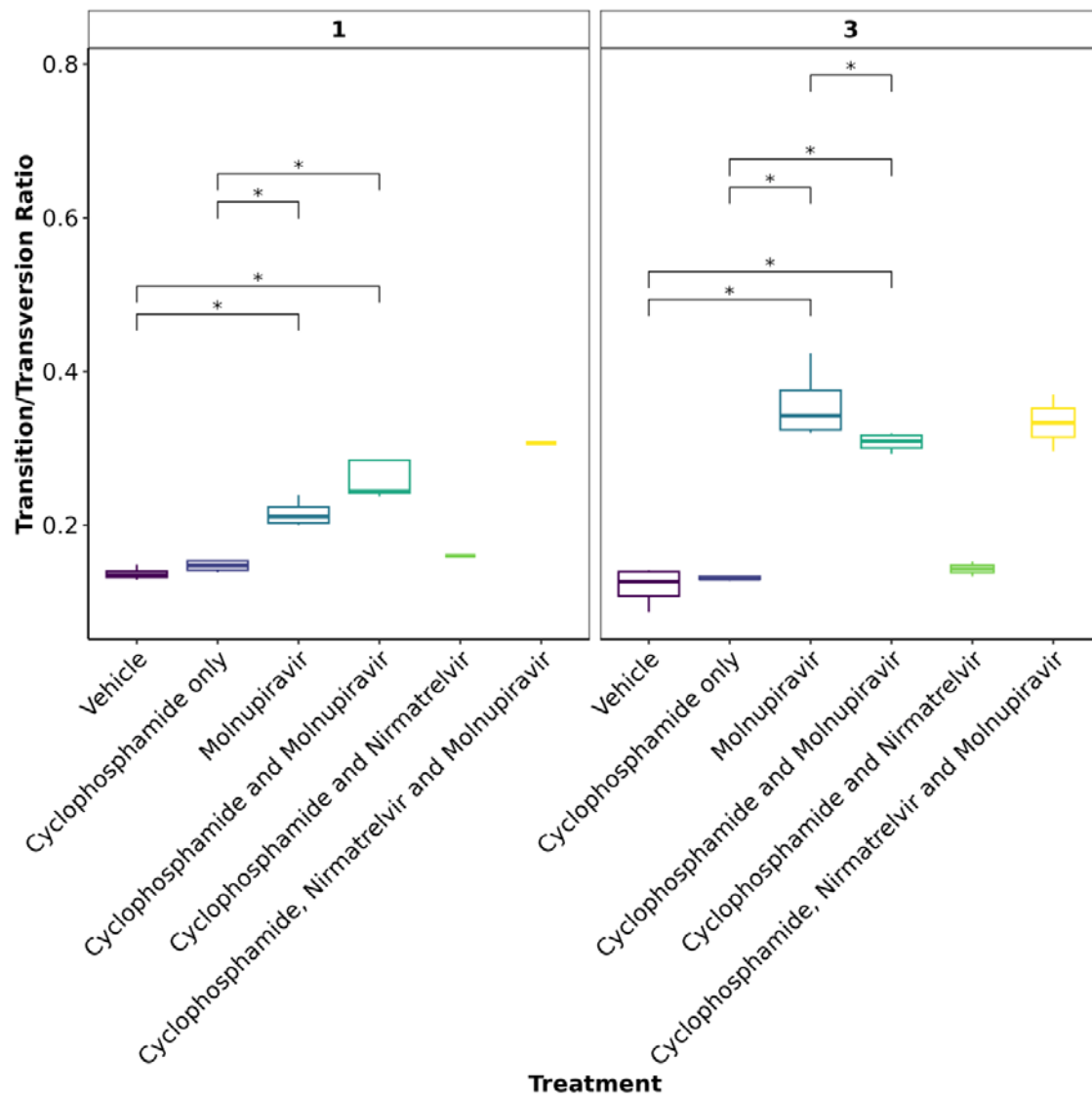
445

446 **Molnupiravir increases the Ts/Tv ratio at the minor variant level in genomes
447 derived from swabs**

448 To further assess the impact of immunocompromising mice by cyclophosphamide,
449 and the therapeutic agents molnupiravir and the nirmatrelvir, a minor variant analysis
450 was conducted on samples derived from throat swabs as performed previously²².
451 Only samples with a >90X coverage with a 100X depth were taken forward into this
452 analysis and the average depth was over 1400 for each sample (Fig S3). No
453 relationship was observed between ct value and the calculated average
454 transition/transversion (Ts/Tv) (Fig S4). The average Ts/Tv ratio for SARS-CoV-2
455 genomes from each mouse and the mean of each group was compared across
456 cohorts at day 1, day 3 and day 5 of infection in line with analysis performed
457 previously in a phase II clinical trial²². On day 1, an increase in Ts/Tv ration was
458 observed in the molnupiravir cohort and the cyclophosphamide and molnupiravir
459 cohort and had a p value < 0.05 when compared to the vehicle control and
460 cyclophosphamide only groups (Fig. 7). The number of samples analysed for
461 cyclophosphamide and nirmatrelvir only was too small for statistical analysis,
462 however, the trend resembles that of vehicle and cyclophosphamide only with little
463 change in the Ts/Tv ratio. Likewise, the combined cyclophosphamide and
464 molnupiravir and nirmatrelvir cohort is represented by one genome derived from one
465 mouse, due to low sequencing coverage obtained from the other mice within this
466 group, however, the trend resembles that of other genomes with exposure to
467 molnupiravir with an increased Ts/Tv ratio. The same is observed at day 3 of
468 sampling, however, there is a significant difference between the mean Ts/Tv ratio
469 between the molnupiravir only and cyclophosphamide and molnupiravir groups.
470 Importantly, the Ts/Tv ratios between the vehicle control and cyclophosphamide only
471 groups resemble each other demonstrating that immunosuppression itself does not
472 drive diversification of the viral genome over this time course. Curiously, when
473 looking at base changes independently of the Ts/Tv ratios, there are significant
474 changes between C to G, C to A and A to U in cyclophosphamide groups on day 1
475 and day 3 (Fig S3). This could be evidence of RNA editing through ROS.
476 Cyclophosphamide has been shown to activate oxidative stress pathways previously
477 and may be a consequence of this treatment^{54,55}. This highlights a research gap in
478 events that can influence RNA editing in RNA viruses. The proportion of base
479 changes in the C to U and G to A transitions were significantly different in the
480 molnupiravir only group as previously seen in a phase II clinical trial²²²³ (Figure 8).

481

482 Further investigations are warranted to understand completely the role of
483 immunocompromised individuals in the development of SARS-CoV-2 variants. It is
484 more likely that immunodeficiency promotes viral persistence providing the virus
485 more opportunity to replicate and introduce mutations. Molnupiravir, compared to
486 nirmatrelvir, shows a stronger mutagenic effect in this model at the minor variant
487 level, however, data is insufficient to make conclusions regards consensus level
488 changes over the timeframes used in this study. When these therapies are used
489 individually or in combination, there is successful depletion in viral load and animals
490 recover from infection, whilst preventing infiltration into brain tissue. Given the
491 concern of molnupiravir associated lineages in circulation ²³, combination therapy
492 may reduce this through more effective clearance of the virus ²⁰, although this would
493 need to be evaluated over time in a real-world setting as the mutational signatures
494 were observed in the combined therapy group. The AGILE clinical trial is currently
495 ongoing to answer this question (ISRCTN: ISRCTN27106947). It is important to
496 note, that the mutational spectrum reported in this study is obtained by amplicon
497 sequencing data, and there is potential for RT-PCR errors within the data.



498

499

500 **Figure 7:** The mean Ts/Tv ratio per genome plotted as boxplots. The plot is faceted by day post infection. Less genomes were recovered for cyclophosphamide and nirmatrelvir and cyclophosphamide, nirmatrelvir and molnupiravir, therefore statistical analysis returns the differences as non-significant. Trends can be concluded with caution. * Represents a P value <0.05 (Mann Whitney U test).

501

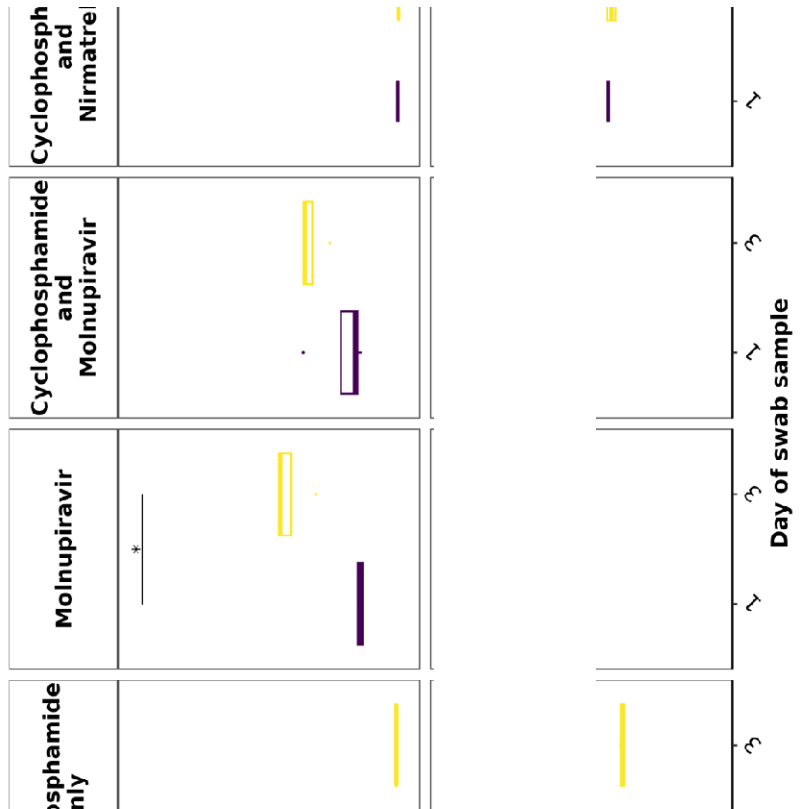
502

503

504

505

506



507
508

509 **Acknowledgements**

510 The authors are grateful to the technical staff at the Histology Laboratory, Institute of
511 Veterinary Pathology, Vetsuisse Faculty, University of Zurich, for excellent technical
512 support. JAH is a member of the ISARIC4C consortium
513 (<https://isaric4c.net/about/authors/>), and we thank them for the use of the SARS-
514 CoV-2 isolate used in this study.

515

516 **Funding**

517 This work was funded by the MRC (MR/W005611/1) 'G2P-UK: A national virology
518 consortium to address phenotypic consequences of SARS-CoV-2 genomic variation'
519 and MR/Y004205/1 'The G2P2 virology consortium: keeping pace with SARS-CoV-2
520 variants, providing evidence to vaccine policy, and building agility for the next
521 pandemic' (co-Is JPS and JAH) and funded in part by U.S. Food and Drug
522 Administration Medical Countermeasures Initiative contract (75F40120C00085) to
523 JAH. The article reflects the views of the authors and does not represent the views
524 or policies of the FDA. Additionally, DNDi under the support by the Wellcome Trust
525 (Grant ref: 222489/Z/21/Z to AO and JPS) through the 'COVID-19 Therapeutics
526 Accelerator'. A.O. acknowledges funding by Wellcome Trust (222489/Z/21/Z),
527 EPSRC (EP/R024804/1; EP/S012265/1) and National Institute of Health (NIH)
528 (R01AI134091; R24AI118397). J.P.S. also acknowledges funding from the Medical
529 Research Council (MRC) (MR/R010145/1, MR/W021641/1, PA6162_G2P2-2023),
530 BBSRC (BB/R00904X/1; BB/R018863/1; BB/N022505/1) and Innovate UK
531 (TS/W022648/1). A.K. received support from the Swiss National Science
532 Foundation (SNSF; IZSEZ0 213289).

533

534 **Transparency Declaration**

535 A.O. is a director of Tandem Nano Ltd and co-inventor of patents relating to drug
536 delivery. A.O. has been co-investigator on funding received by the University of
537 Liverpool from ViiV Healthcare and Gilead Sciences in the past 3 years unrelated to
538 COVID-19. A.O. has received personal fees from Gilead and Assembly Biosciences
539 in the past 3 years, also unrelated to COVID-19. JPS has received funding from ENA
540 respiratory Pty Ltd, Bicycle Tx Ltd, and Infex Therapeutics Ltd unrelated to this
541 study. R.P.R. is an employee at TopMD Precision Medicine Ltd. No other conflicts
542 are declared by the authors.

543 **References**

544 1 Moore, S. C., Penrice-Randal, R., Alruwaili, M., Randle, N., Armstrong, S., Hartley, C.,
545 Haldenby, S., Dong, X., Alrezaihi, A., Almsaud, M., Bentley, E., Clark, J., Garcia-
546 Dorival, I., Gilmore, P., Han, X., Jones, B., Luu, L., Sharma, P., Shawli, G., Sun, Y., Zhao,
547 Q., Pullan, S. T., Carter, D. P., Bewley, K., Dunning, J., Zhou, E. M., Solomon, T.,
548 Beadsworth, M., Cruise, J., Crook, D. W., Matthews, D. A., Davidson, A. D.,
549 Mahmood, Z., Aljabr, W., Druce, J., Vipond, R., Ng, L., Renia, L., Openshaw, P. J. M.,
550 Baillie, J. K., Carroll, M. W., Stewart, J., Darby, A., Semple, M., Turtle, L. & Hiscox, J. A.
551 Amplicon-Based Detection and Sequencing of SARS-CoV-2 in Nasopharyngeal Swabs
552 from Patients With COVID-19 and Identification of Deletions in the Viral Genome
553 That Encode Proteins Involved in Interferon Antagonism. *Viruses* **12** (2020).
554 <https://doi.org/10.3390/v12101164>

555 2 McCarthy, K. R., Rennick, L. J., Nambulli, S., Robinson-McCarthy, L. R., Bain, W. G.,
556 Haidar, G. & Duprex, W. P. Natural deletions in the SARS-CoV-2 spike glycoprotein
557 drive antibody escape. *bioRxiv*, 2020.2011.2019.389916 (2020).
558 <https://doi.org/10.1101/2020.11.19.389916>

559 3 Korber, B., Fischer, W. M., Gnanakaran, S., Yoon, H., Theiler, J., Abfalterer, W.,
560 Hengartner, N., Giorgi, E. E., Bhattacharya, T., Foley, B., Hastie, K. M., Parker, M. D.,
561 Partridge, D. G., Evans, C. M., Freeman, T. M., de Silva, T. I., Sheffield, C.-G. G.,
562 McDanal, C., Perez, L. G., Tang, H., Moon-Walker, A., Whelan, S. P., LaBranche, C. C.,
563 Saphire, E. O. & Montefiori, D. C. Tracking Changes in SARS-CoV-2 Spike: Evidence
564 that D614G Increases Infectivity of the COVID-19 Virus. *Cell* **182**, 812-827 e819
565 (2020). <https://doi.org/10.1016/j.cell.2020.06.043>

566 4 Alruwaili, M., Armstrong, S., Prince, T., Erdmann, M., Matthews, D. A., Luu, L.,
567 Davidson, A., Aljabr, W. & Hiscox, J. A. SARS-CoV-2 NSP12 associates with TRiC and
568 the P323L substitution acts as a host adaption. *Journal of virology* **97**, e0042423
569 (2023). <https://doi.org/10.1128/jvi.00424-23>

570 5 Goldswain, H., Dong, X., Penrice-Randal, R., Alruwaili, M., Shawli, G. T., Prince, T.,
571 Williamson, M. K., Raghwani, J., Randle, N., Jones, B., Donovan-Banfield, I. a.,
572 Salguero, F. J., Tree, J. A., Hall, Y., Hartley, C., Erdmann, M., Bazire, J.,
573 Jearanaiwitayakul, T., Semple, M. G., Openshaw, P. J. M., Baillie, J. K., Baillie, J. K.,
574 Semple, M. G., Openshaw, P. J. M., Carson, G., Alex, B., Andrikopoulos, P., Bach, B.,
575 Barclay, W. S., Bogaert, D., Chand, M., Chechi, K., Cooke, G. S., da Silva Filipe, A., de
576 Silva, T., Docherty, A. B., dos Santos Correia, G., Dumas, M.-E., Dunning, J., Fletcher,
577 T., Green, C. A., Greenhalf, W., Griffin, J. L., Gupta, R. K., Harrison, E. M., Hiscox, J. A.,
578 Ho, A. Y. W., Horby, P. W., Ijaz, S., Khoo, S., Klenerman, P., Law, A., Lewis, M. R., Liggi,
579 S., Lim, W. S., Maslen, L., Mentzer, A. J., Merson, L., Meynert, A. M., Moore, S. C.,
580 Noursadeghi, M., Olanipekun, M., Osagie, A., Palmarini, M., Palmieri, C., Paxton, W.
581 A., Pollakis, G., Price, N., Rambaut, A., Robertson, D. L., Russell, C. D., Sancho-
582 Shimizu, V., Sands, C. J., Scott, J. T., Sigfrid, L., Solomon, T., Sriskandan, S., Stuart, D.,
583 Summers, C., Swann, O. V., Takats, Z., Takis, P., Tedder, R. S., Thompson, A. A. R.,
584 Thomson, E. C., Thwaites, R. S., Turtle, L. C. W., Zambon, M., Hardwick, H., Donohue,
585 C., Griffiths, F., Oosthuyzen, W., Donegan, C., Spencer, R. G., Norman, L., Pius, R.,
586 Drake, T. M., Fairfield, C. J., Knight, S. R., McLean, K. A., Murphy, D., Shaw, C. A.,
587 Dalton, J., Girvan, M., Saviciute, E., Roberts, S., Harrison, J., Marsh, L., Connor, M.,
588 Halpin, S., Jackson, C., Gamble, C., Plotkin, D., Lee, J., Leeming, G., Law, A., Wham,
589 M., Clohisey, S., Hendry, R., Scott-Brown, J., Shaw, V., McDonald, S. E., Keating, S.,

590 Ahmed, K. A., Armstrong, J. A., Ashworth, M., Asiimwe, I. G., Bakshi, S., Barlow, S. L.,
591 Booth, L., Brennan, B., Bullock, K., Catterall, B. W. A., Clark, J. J., Clarke, E. A., Cole, S.,
592 Cooper, L., Cox, H., Davis, C., Dincarslan, O., Dunn, C., Dyer, P., Elliott, A., Evans, A.,
593 Finch, L., Fisher, L. W. S., Foster, T., Garcia-Dorival, I., Gunning, P., Jensen, R. L.,
594 Jones, C. B., Jones, T. R., Khandaker, S., King, K., Kiy, R. T., Koukorava, C., Lake, A.,
595 Lant, S., Latawiec, D., Lavelle-Langham, L., Lefteri, D., Lett, L., Livoti, L. A., Mancini,
596 M., McDonald, S., McEvoy, L., McLauchlan, J., Metelmann, S., Miah, N. S., Middleton,
597 J., Mitchell, J., Moore, S. C., Murphy, E. G., Pilgrim, J., Reynolds, W., Ridley, P. M.,
598 Sales, D., Shaw, V. E., Shears, R. K., Small, B., Subramaniam, K. S., Szemiel, A.,
599 Taggart, A., Tanianis-Hughes, J., Thomas, J., Trochu, E., van Tonder, L., Wilcock, E.,
600 Zhang, J. E., Flaherty, L., Maziere, N., Cass, E., Carracedo, A. D., Carlucci, N., Holmes,
601 A., Massey, H., Murphy, L., McCafferty, S., Clark, R., Fawkes, A., Morrice, K., Maclean,
602 A., Wrobel, N., Donnelly, L., Coutts, A., Hafezi, K., MacGillivray, L., Gilchrist, T.,
603 Adeniji, K., Agranoff, D., Agwu, K., Ail, D., Aldera, E. L., Alegria, A., Allen, S., Angus,
604 B., Ashish, A., Atkinson, D., Bari, S., Barlow, G., Barnass, S., Barrett, N., Bassford, C.,
605 Basude, S., Baxter, D., Beadsworth, M., Bernatoniene, J., Berridge, J., Berry, C., Best,
606 N., Bothma, P., Chadwick, D., Brittain-Long, R., Bulteel, N., Burden, T., Burtenshaw,
607 A., Caruth, V., Chadwick, D., Chamberl, D., Chee, N., Child, J., Chukkambotla, S., Clark,
608 T., Collini, P., Cosgrove, C., Cupitt, J., Cutino-Moguel, M.-T., Dark, P., Dawson, C.,
609 Dervisevic, S., Donnison, P., Douthwaite, S., Drummond, A., DuRand, I., Dushianthan,
610 A., Dyer, T., Evans, C., Eziefula, C., Fegan, C., Finn, A., Fullerton, D., Garg, S., Garg, S.,
611 Garg, A., Gkrania-Klotsas, E., Godden, J., Goldsmith, A., Graham, C., Hardy, E.,
612 Hartshorn, S., Harvey, D., Havalda, P., Hawcutt, D. B., Hobrok, M., Hodgson, L.,
613 Hormis, A., Jacobs, M., Jain, S., Jennings, P., Kaliappan, A., Kasipandian, V., Kegg, S.,
614 Kelsey, M., Kendall, J., Kerrison, C., Kerslake, I., Koch, O., Koduri, G., Koshy, G., Laha,
615 S., Laird, S., Larkin, S., Leiner, T., Lillie, P., Limb, J., Linnett, V., Little, J., Lyttle, M.,
616 MacMahon, M. & Investigators, I. C. The P323L substitution in the SARS-CoV-2
617 polymerase (NSP12) confers a selective advantage during infection. *Genome Biology*
618 **24**, 47 (2023). <https://doi.org/10.1186/s13059-023-02881-5>

619 6 Wang, B., Goh, Y. S., Prince, T., Ngoh, E. Z. X., Salleh, S. N. M., Hor, P. X., Loh, C. Y.,
620 Fong, S. W., Hartley, C., Tan, S. Y., Young, B. E., Leo, Y. S., Lye, D. C., Maurer-Stroh, S.,
621 Ng, L. F. P., Hiscox, J. A., Renia, L. & Wang, C. I. Resistance of SARS-CoV-2 variants to
622 neutralization by convalescent plasma from early COVID-19 outbreak in Singapore.
623 *NPJ Vaccines* **6**, 125 (2021). <https://doi.org/10.1038/s41541-021-00389-2>

624 7 Suzuki, R., Yamasoba, D., Kimura, I., Wang, L., Kishimoto, M., Ito, J., Morioka, Y., Nao,
625 N., Nasser, H., Uriu, K., Kosugi, Y., Tsuda, M., Orba, Y., Sasaki, M., Shimizu, R.,
626 Kawabata, R., Yoshimatsu, K., Asakura, H., Nagashima, M., Sadamasu, K., Yoshimura,
627 K., Genotype to Phenotype Japan, C., Sawa, H., Ikeda, T., Irie, T., Matsuno, K.,
628 Tanaka, S., Fukuhara, T. & Sato, K. Attenuated fusogenicity and pathogenicity of
629 SARS-CoV-2 Omicron variant. *Nature* **603**, 700-705 (2022).
630 <https://doi.org/10.1038/s41586-022-04462-1>

631 8 Corey, L., Beyrer, C., Cohen, M. S., Michael, N. L., Bedford, T. & Rolland, M. SARS-
632 CoV-2 Variants in Patients with Immunosuppression. *N Engl J Med* **385**, 562-566
633 (2021). <https://doi.org/10.1056/NEJMsb2104756>

634 9 Avanzato, V. A., Matson, M. J., Seifert, S. N., Pryce, R., Williamson, B. N., Anzick, S. L.,
635 Barbian, K., Judson, S. D., Fischer, E. R., Martens, C., Bowden, T. A., de Wit, E., Riedo,
636 F. X. & Munster, V. J. Case Study: Prolonged Infectious SARS-CoV-2 Shedding from an

637 Asymptomatic Immunocompromised Individual with Cancer. *Cell* **183**, 1901-1912
638 e1909 (2020). <https://doi.org/10.1016/j.cell.2020.10.049>

639 10 Young, B. E., Fong, S. W., Chan, Y. H., Mak, T. M., Ang, L. W., Anderson, D. E., Lee, C.
640 Y., Amrun, S. N., Lee, B., Goh, Y. S., Su, Y. C. F., Wei, W. E., Kalimuddin, S., Chai, L. Y.
641 A., Pada, S., Tan, S. Y., Sun, L., Parthasarathy, P., Chen, Y. Y. C., Barkham, T., Lin, R. T.
642 P., Maurer-Stroh, S., Leo, Y. S., Wang, L. F., Renia, L., Lee, V. J., Smith, G. J. D., Lye, D.
643 C. & Ng, L. F. P. Effects of a major deletion in the SARS-CoV-2 genome on the severity
644 of infection and the inflammatory response: an observational cohort study. *Lancet*
645 **396**, 603-611 (2020). [https://doi.org/10.1016/S0140-6736\(20\)31757-8](https://doi.org/10.1016/S0140-6736(20)31757-8)

646 11 Aljabr, W., Alruwaili, M., Penrice-Randal, R., Alrezaihi, A., Harrison, A. J., Ryan, Y.,
647 Bentley, E., Jones, B., Alhatlani, B. Y., AlShahrani, D., Mahmood, Z., Rickett, N. Y.,
648 Alosaimi, B., Naeem, A., Alamri, S., Alsran, H., Hamed, M. E., Dong, X., Assiri, A. M.,
649 Alrasheed, A. R., Hamza, M., Carroll, M. W., Gemmell, M., Darby, A., Donovan-
650 Banfield, I., Stewart, J. P., Matthews, D. A., Davidson, A. D. & Hiscox, J. A. Amplicon
651 and Metagenomic Analysis of Middle East Respiratory Syndrome (MERS) Coronavirus
652 and the Microbiome in Patients with Severe MERS. *mSphere* **6**, e0021921 (2021).
653 <https://doi.org/10.1128/mSphere.00219-21>

654 12 Chu, D. K. W., Hui, K. P. Y., Perera, R., Miguel, E., Niemeyer, D., Zhao, J.,
655 Channappanavar, R., Dudas, G., Oladipo, J. O., Traore, A., Fassi-Fihri, O., Ali, A.,
656 Demissie, G. F., Muth, D., Chan, M. C. W., Nicholls, J. M., Meyerholz, D. K., Kuranga,
657 S. A., Mamo, G., Zhou, Z., So, R. T. Y., Hemida, M. G., Webby, R. J., Roger, F.,
658 Rambaut, A., Poon, L. L. M., Perlman, S., Drosten, C., Chevalier, V. & Peiris, M. MERS
659 coronaviruses from camels in Africa exhibit region-dependent genetic diversity. *Proc
660 Natl Acad Sci U S A* **115**, 3144-3149 (2018).
661 <https://doi.org/10.1073/pnas.1718769115>

662 13 El-Kafrawy, S. A., Corman, V. M., Tolah, A. M., Al Masaudi, S. B., Hassan, A. M.,
663 Muller, M. A., Bleicker, T., Harakeh, S. M., Alzahrani, A. A., Alsaaidi, G. A., Alagili, A.
664 N., Hashem, A. M., Zumla, A., Drosten, C. & Azhar, E. I. Enzootic patterns of Middle
665 East respiratory syndrome coronavirus in imported African and local Arabian
666 dromedary camels: a prospective genomic study. *Lancet Planet Health* **3**, e521-e528
667 (2019). [https://doi.org/10.1016/S2542-5196\(19\)30243-8](https://doi.org/10.1016/S2542-5196(19)30243-8)

668 14 Rottier, P. J., Nakamura, K., Schellen, P., Volders, H. & Hajema, B. J. Acquisition of
669 macrophage tropism during the pathogenesis of feline infectious peritonitis is
670 determined by mutations in the feline coronavirus spike protein. *Journal of virology*
671 **79**, 14122-14130 (2005). <https://doi.org/10.1128/jvi.79.22.14122-14130.2005>

672 15 Licita, B. N., Millet, J. K., Regan, A. D., Hamilton, B. S., Rinaldi, V. D., Duhamel, G. E.
673 & Whittaker, G. R. Mutation in spike protein cleavage site and pathogenesis of feline
674 coronavirus. *Emerg Infect Dis* **19**, 1066-1073 (2013).
675 <https://doi.org/10.3201/eid1907.121094>

676 16 Vennema, H., Poland, A., Foley, J. & Pedersen, N. C. Feline infectious peritonitis
677 viruses arise by mutation from endemic feline enteric coronaviruses. *Virology* **243**,
678 150-157 (1998). <https://doi.org/10.1006/viro.1998.9045>

679 17 Kipar, A., Meli, M. L., Baptiste, K. E., Bowker, L. J. & Lutz, H. Sites of feline
680 coronavirus persistence in healthy cats. *The Journal of general virology* **91**, 1698-
681 1707 (2010). <https://doi.org/10.1099/vir.0.020214-0>

682 18 Li, P., Wang, Y., Lavrijzen, M., Lamers, M. M., de Vries, A. C., Rottier, R. J., Bruno, M.
683 J., Peppelenbosch, M. P., Haagmans, B. L. & Pan, Q. SARS-CoV-2 Omicron variant is

684 highly sensitive to molnupiravir, nirmatrelvir, and the combination. *Cell Res* **32**, 322-
685 324 (2022). <https://doi.org/10.1038/s41422-022-00618-w>

686 19 Gidari, A., Sabbatini, S., Schiaroli, E., Bastianelli, S., Pierucci, S., Busti, C., Comez, L.,
687 Libera, V., Macchiarulo, A., Paciaroni, A., Vicenti, I., Zazzi, M. & Francisci, D. The
688 Combination of Molnupiravir with Nirmatrelvir or GC376 Has a Synergic Role in the
689 Inhibition of SARS-CoV-2 Replication In Vitro. *Microorganisms* **10** (2022).
690 <https://doi.org/10.3390/microorganisms10071475>

691 20 Hiscox, J. A., Khoo, S. H., Stewart, J. P. & Owen, A. Shutting the gate before the horse
692 has bolted: is it time for a conversation about SARS-CoV-2 and antiviral drug
693 resistance? *J Antimicrob Chemother* **76**, 2230-2233 (2021).
694 <https://doi.org/10.1093/jac/dkab189>

695 21 Szemiel, A. M., Merits, A., Orton, R. J., MacLean, O. A., Pinto, R. M., Wickenhagen, A.,
696 Lieber, G., Turnbull, M. L., Wang, S., Furnon, W., Suarez, N. M., Mair, D., da Silva
697 Filipe, A., Willett, B. J., Wilson, S. J., Patel, A. H., Thomson, E. C., Palmarini, M., Kohl,
698 A. & Stewart, M. E. In vitro selection of Remdesivir resistance suggests evolutionary
699 predictability of SARS-CoV-2. *PLoS Pathog* **17**, e1009929 (2021).
700 <https://doi.org/10.1371/journal.ppat.1009929>

701 22 Donovan-Banfield, I. a., Penrice-Randal, R., Goldswain, H., Rzeszutek, A. M., Pilgrim,
702 J., Bullock, K., Saunders, G., Northey, J., Dong, X. & Ryan, Y. Characterisation of SARS-
703 CoV-2 genomic variation in response to molnupiravir treatment in the AGILE Phase
704 IIa clinical trial. *Nature Communications* **13**, 7284-7284 (2022).

705 23 Sanderson, T., Hisner, R., Donovan-Banfield, I. a., Hartman, H., Løchen, A., Peacock,
706 T. P. & Ruis, C. A molnupiravir-associated mutational signature in global SARS-CoV-2
707 genomes. *Nature* **623**, 594-600 (2023). <https://doi.org/10.1038/s41586-023-06649-6>

708 24 Li, P., de Vries, A. C., Kamar, N., Peppelenbosch, M. P. & Pan, Q. Monitoring and
709 managing SARS-CoV-2 evolution in immunocompromised populations. *Lancet
710 Microbe* **3**, e325-e326 (2022). [https://doi.org/10.1016/S2666-5247\(22\)00061-1](https://doi.org/10.1016/S2666-5247(22)00061-1)

711 25 Bentley, E. G., Kirby, A., Sharma, P., Kipar, A., Mega, D. F., Bramwell, C., Penrice-
712 Randal, R., Prince, T., Brown, J. C., Zhou, J., Screamton, G. R., Barclay, W. S., Owen, A.,
713 Hiscox, J. A. & Stewart, J. P. SARS-CoV-2 Omicron-B.1.1.529 Variant leads to less
714 severe disease than Pango B and Delta variants strains in a mouse model of severe
715 COVID-19. *bioRxiv*, 2021.2012.2026.474085 (2021).
716 <https://doi.org/10.1101/2021.12.26.474085>

717 26 Clark, J. J., Penrice-Randal, R., Sharma, P., Kipar, A., Dong, X., Pennington, S. H.,
718 Marriott, A. E., Colombo, S., Davidson, A., Williamson, M. K., Matthews, D. A., Turtle,
719 L., Prince, T., Hughes, G. L., Patterson, E. I., Shawli, G., Mega, D. F., Subramaniam, K.,
720 Sharp, J., McLaughlin, L., Zhou, E.-M., Turner, J. D., Biagini, G., Owen, A., Hiscox, J. A.
721 & Stewart, J. P. Sequential infection with influenza A virus followed by severe acute
722 respiratory syndrome coronavirus 2 (SARS-CoV-2) leads to more severe disease and
723 encephalitis in a mouse model of COVID-19. *bioRxiv*, 2020.2010.2013.334532 (2023).
724 <https://doi.org/10.1101/2020.10.13.334532>

725 27 Gaynor, K. U., Vaysburd, M., Harman, M. A. J., Albecka, A., Jeffrey, P., Beswick, P.,
726 Papa, G., Chen, L., Mallery, D., McGuinness, B., Van Rietschoten, K., Stanway, S.,
727 Brear, P., Lulla, A., Ciazynska, K., Chang, V. T., Sharp, J., Neary, M., Box, H., Herriott,
728 J., Kijak, E., Tatham, L., Bentley, E. G., Sharma, P., Kirby, A., Han, X., Stewart, J. P.,
729 Owen, A., Briggs, J. A. G., Hyvönen, M., Skynner, M. J. & James, L. C. Multivalent
730 bicyclic peptides are an effective antiviral modality that can potently inhibit SARS-

731 28 CoV-2. *Nature Communications* **14**, 3583 (2023). <https://doi.org/10.1038/s41467-023-39158-1>

732 28 Russell, C. D., Valanciute, A., Gachanja, N. N., Stephen, J., Penrice-Randal, R., Armstrong, S. D., Clohisey, S., Wang, B., Al Qsous, W., Wallace, W. A., Oniscu, G. C., Stevens, J., Harrison, D. J., Dhaliwal, K., Hiscox, J. A., Baillie, J. K., Akram, A. R., Dorward, D. A. & Lucas, C. D. Tissue Proteomic Analysis Identifies Mechanisms and Stages of Immunopathology in Fatal COVID-19. *Am J Respir Cell Mol Biol* (2021). <https://doi.org/10.1165/rccm.2021-0358OC>

733 29 Dorward, D. A., Russell, C. D., Um, I. H., Elshani, M., Armstrong, S. D., Penrice-Randal, R., Millar, T., Lerpiniere, C. E. B., Tagliavini, G., Hartley, C. S., Randle, N. P., Gachanja, N. N., Potey, P. M. D., Dong, X., Anderson, A. M., Campbell, V. L., Duguid, A. J., Al Qsous, W., BouHaidar, R., Baillie, J. K., Dhaliwal, K., Wallace, W. A., Bellamy, C. O. C., Prost, S., Smith, C., Hiscox, J. A., Harrison, D. J. & Lucas, C. D. Tissue-Specific Immunopathology in Fatal COVID-19. *Am J Respir Crit Care Med* **203**, 192-201 (2021). <https://doi.org/10.1164/rccm.202008-3265OC>

734 30 Patterson, E. I., Prince, T., Anderson, E. R., Casas-Sanchez, A., Smith, S. L., Cansado-Utrilla, C., Solomon, T., Griffiths, M. J., Acosta-Serrano, A., Turtle, L. & Hughes, G. L. Methods of Inactivation of SARS-CoV-2 for Downstream Biological Assays. *J Infect Dis* **222**, 1462-1467 (2020). <https://doi.org/10.1093/infdis/jiaa507>

735 31 Davidson, A. D., Williamson, M. K., Lewis, S., Shoemark, D., Carroll, M. W., Heesom, K. J., Zambon, M., Ellis, J., Lewis, P. A., Hiscox, J. A. & Matthews, D. A. Characterisation of the transcriptome and proteome of SARS-CoV-2 reveals a cell passage induced in-frame deletion of the furin-like cleavage site from the spike glycoprotein. *Genome Med* **12**, 68 (2020).

736 32 Abdelnabi, R., Foo, C. S., Kaptein, S. J. F., Boudewijns, R., Vangeel, L., Jonghe, S. D., Jochmans, D., Weynand, B. & Neyts, J. A SCID Mouse Model To Evaluate the Efficacy of Antivirals against SARS-CoV-2 Infection. *Journal of virology* **96**, e00758-00722 (2022). <https://doi.org/doi:10.1128/jvi.00758-22>

737 33 Jeong, J. H., Chokkakula, S., Min, S. C., Kim, B. K., Choi, W.-S., Oh, S., Yun, Y. S., Kang, D. H., Lee, O.-J., Kim, E.-G., Choi, J.-H., Lee, J.-Y., Choi, Y. K., Baek, Y. H. & Song, M.-S. Combination therapy with nirmatrelvir and molnupiravir improves the survival of SARS-CoV-2 infected mice. *Antiviral Research* **208**, 105430 (2022). <https://doi.org/https://doi.org/10.1016/j.antiviral.2022.105430>

738 34 Wahl, A., Gralinski, L. E., Johnson, C. E., Yao, W., Kovarova, M., Dinnon, K. H., Liu, H., Madden, V. J., Krzystek, H. M., De, C., White, K. K., Gully, K., Schäfer, A., Zaman, T., Leist, S. R., Grant, P. O., Bluemling, G. R., Kolykhalov, A. A., Natchus, M. G., Askin, F. B., Painter, G., Browne, E. P., Jones, C. D., Pickles, R. J., Baric, R. S. & Garcia, J. V. SARS-CoV-2 infection is effectively treated and prevented by EIDD-2801. *Nature* **591**, 451-457 (2021). <https://doi.org/10.1038/s41586-021-03312-w>

739 35 Stegmann, K. M., Dickmanns, A., Heinen, N., Blaurock, C., Karrasch, T., Breithaupt, A., Klopferleisch, R., Uhlig, N., Eberlein, V., Issmail, L., Herrmann, S. T., Schreieck, A., Peelen, E., Kohlhof, H., Sadeghi, B., Riek, A., Speakman, J. R., Groß, U., Görlich, D., Vitt, D., Müller, T., Grunwald, T., Pfaender, S., Balkema-Buschmann, A. & Dobbelstein, M. Inhibitors of dihydroorotate dehydrogenase cooperate with molnupiravir and N4-hydroxycytidine to suppress SARS-CoV-2 replication. *iScience* **25**, 104293 (2022). <https://doi.org/https://doi.org/10.1016/j.isci.2022.104293>

777 36 De Neck, S., Penrice-Randal, R., Clark, J. J., Sharma, P., Bentley, E. G., Kirby, A., Mega, D. F., Han, X., Owen, A., Hiscox, J. A., Stewart, J. P. & Kipar, A. The Stereotypic Response of the Pulmonary Vasculature to Respiratory Viral Infections: Findings in Mouse Models of SARS-CoV-2, Influenza A and Gammaherpesvirus Infections. *Viruses* **15** (2023).

782 37 Seehusen, F., Clark, J. J., Sharma, P., Bentley, E. G., Kirby, A., Subramaniam, K., Wunderlin-Giuliani, S., Hughes, G. L., Patterson, E. I., Michael, B. D., Owen, A., Hiscox, J. A., Stewart, J. P. & Kipar, A. Neuroinvasion and Neurotropism by SARS-CoV-2 Variants in the K18-hACE2 Mouse. *Viruses* **14** (2022). <https://doi.org/10.3390/v14051020>

787 38 Coolen, J. P. M., Wolters, F., Tostmann, A., van Groningen, L. F. J., Bleeker-Rovers, C. P., Tan, E. C. T. H., van der Geest-Blankert, N., Hautvast, J. L. A., Hopman, J., Wertheim, H. F. L., Rahamat-Langendoen, J. C., Storch, M. & Melchers, W. J. G. SARS-CoV-2 whole-genome sequencing using reverse complement PCR: For easy, fast and accurate outbreak and variant analysis. *Journal of Clinical Virology* **144**, 104993 (2021). <https://doi.org/https://doi.org/10.1016/j.jcv.2021.104993>

793 39 Avanzato, V. A., Matson, M. J., Seifert, S. N., Pryce, R., Williamson, B. N., Anzick, S. L., Barbian, K., Judson, S. D., Fischer, E. R., Martens, C., Bowden, T. A., de Wit, E., Riedo, F. X. & Munster, V. J. Case Study: Prolonged Infectious SARS-CoV-2 Shedding from an Asymptomatic Immunocompromised Individual with Cancer. *Cell* **183**, 1901-1912.e1909 (2020). <https://doi.org/10.1016/j.cell.2020.10.049>

798 40 Burki, T. The origin of SARS-CoV-2 variants of concern. *Lancet Infect Dis* **22**, 174-175 (2022). [https://doi.org/10.1016/s1473-3099\(22\)00015-9](https://doi.org/10.1016/s1473-3099(22)00015-9)

800 41 Caccuri, F., Messali, S., Bortolotti, D., Di Silvestre, D., De Palma, A., Cattaneo, C., Bertelli, A., Zani, A., Milanesi, M., Giovanetti, M., Campisi, G., Gentili, V., Bugatti, A., Filippini, F., Scaltriti, E., Pongolini, S., Tucci, A., Fiorentini, S., d'Ursi, P., Ciccozzi, M., Mauri, P., Rizzo, R. & Caruso, A. Competition for dominance within replicating quasispecies during prolonged SARS-CoV-2 infection in an immunocompromised host. *Virus Evol* **8**, veac042 (2022). <https://doi.org/10.1093/ve/veac042>

806 42 Chen, L., Zody, M. C., Di Germanio, C., Martinelli, R., Mediavilla, J. R., Cunningham, M. H., Composto, K., Chow, K. F., Kordalewska, M., Corvelo, A., Oschwald, D. M., Fennessey, S., Zetkulic, M., Dar, S., Kramer, Y., Mathema, B., Germer, S., Stone, M., Simmons, G., Busch, M. P., Maniatis, T., Perlin, D. S. & Kreiswirth, B. N. Emergence of Multiple SARS-CoV-2 Antibody Escape Variants in an Immunocompromised Host Undergoing Convalescent Plasma Treatment. *mSphere* **6**, e0048021 (2021). <https://doi.org/10.1128/mSphere.00480-21>

813 43 Choi, B., Choudhary, M. C., Regan, J., Sparks, J. A., Padera, R. F., Qiu, X., Solomon, I. H., Kuo, H.-H., Boucau, J., Bowman, K., Adhikari, U. D., Winkler, M. L., Mueller, A. A., Hsu, T. Y. T., Desjardins, M., Baden, L. R., Chan, B. T., Walker, B. D., Lichtenfeld, M., Brigl, M., Kwon, D. S., Kanjilal, S., Richardson, E. T., Jonsson, A. H., Alter, G., Barczak, A. K., Hanage, W. P., Yu, X. G., Gaiha, G. D., Seaman, M. S., Cernadas, M. & Li, J. Z. Persistence and Evolution of SARS-CoV-2 in an Immunocompromised Host. *New England Journal of Medicine* **383**, 2291-2293 (2020). <https://doi.org/10.1056/NEJMc2031364>

821 44 Peng, K. W., Myers, R., Greenslade, A., Mader, E., Greiner, S., Federspiel, M. J., Dispenzieri, A. & Russell, S. J. Using clinically approved cyclophosphamide regimens

823 to control the humoral immune response to oncolytic viruses. *Gene Therapy* **20**, 255-
824 261 (2013). <https://doi.org/10.1038/gt.2012.31>

825 45 Schaecher, S. R., Stabenow, J., Oberle, C., Schriewer, J., Buller, R. M., Sagartz, J. E. &
826 Pekosz, A. An immunosuppressed Syrian golden hamster model for SARS-CoV
827 infection. *Virology* **380**, 312-321 (2008). <https://doi.org/10.1016/j.virol.2008.07.026>

828 46 Ramasamy, S., Kolloli, A., Kumar, R., Husain, S., Soteropoulos, P., Chang, T. L. &
829 Subbian, S. Comprehensive Analysis of Disease Pathology in Immunocompetent and
830 Immunocompromised Hosts following Pulmonary SARS-CoV-2 Infection.
831 *Biomedicines* **10**, 1343 (2022).

832 47 Brocato, R. L., Principe, L. M., Kim, R. K., Zeng, X., Williams, J. A., Liu, Y., Li, R., Smith,
833 J. M., Golden, J. W., Gangemi, D., Youssef, S., Wang, Z., Glanville, J. & Hooper, J. W.
834 Disruption of Adaptive Immunity Enhances Disease in SARS-CoV-2-Infected Syrian
835 Hamsters. *J Virol* **94** (2020). <https://doi.org/10.1128/jvi.01683-20>

836 48 Salzer, R., Clark, J. J., Vaysburd, M., Chang, V. T., Albecka, A., Kiss, L., Sharma, P.,
837 Gonzalez Llamazares, A., Kipar, A., Hiscox, J. A., Owen, A., Aricescu, A. R., Stewart, J.
838 P., James, L. C. & Lowe, J. Single-dose immunisation with a multimerised SARS-CoV-2
839 receptor binding domain (RBD) induces an enhanced and protective response in
840 mice. *FEBS Lett* **595**, 2323-2340 (2021). <https://doi.org/10.1002/1873-3468.14171>

841 49 Legebeke, J., Lord, J., Penrice-Randal, R., Vallejo, A. F., Poole, S., Brendish, N. J.,
842 Dong, X., Hartley, C., Holloway, J. W., Lucas, J. S., Williams, A. P., Wheway, G.,
843 Strazzeri, F., Gardner, A., Schofield, J. P. R., Skipp, P. J., Hiscox, J. A., Polak, M. E.,
844 Clark, T. W. & Baralle, D. Evaluating the Immune Response in Treatment-Naive
845 Hospitalised Patients With Influenza and COVID-19. *Front Immunol* **13**, 853265
846 (2022). <https://doi.org/10.3389/fimmu.2022.853265>

847 50 Escalera, A., Gonzalez-Reiche, A. S., Aslam, S., Mena, I., Laporte, M., Pearl, R. L.,
848 Fossati, A., Rathnasinghe, R., Alshammary, H., van de Guchte, A., Farrugia, K., Qin, Y.,
849 Bouhaddou, M., Kehrer, T., Zuliani-Alvarez, L., Meekins, D. A., Balaraman, V.,
850 McDowell, C., Richt, J. A., Bajic, G., Sordillo, E. M., Dejosez, M., Zwaka, T. P., Krogan,
851 N. J., Simon, V., Albrecht, R. A., van Bakel, H., García-Sastre, A. & Aydillo, T.
852 Mutations in SARS-CoV-2 variants of concern link to increased spike cleavage and
853 virus transmission. *Cell Host Microbe* **30**, 373-387.e377 (2022).
854 <https://doi.org/10.1016/j.chom.2022.01.006>

855 51 Braun, K. M., Moreno, G. K., Halfmann, P. J., Hodcroft, E. B., Baker, D. A., Boehm, E.
856 C., Weiler, A. M., Haj, A. K., Hatta, M., Chiba, S., Maemura, T., Kawaoka, Y., Koelle, K.,
857 O'Connor, D. H. & Friedrich, T. C. Transmission of SARS-CoV-2 in domestic cats
858 imposes a narrow bottleneck. *PLOS Pathogens* **17**, e1009373 (2021).
859 <https://doi.org/10.1371/journal.ppat.1009373>

860 52 Mizuki, Y., Keiko, T., Youko, H., Jun-ichiro, I., Yasushi, K. & Jin, G. SARS-CoV-2
861 Omicron spike H655Y mutation is responsible for enhancement of the endosomal
862 entry pathway and reduction of cell surface entry pathways. *bioRxiv*,
863 2022.2003.2021.485084 (2022). <https://doi.org/10.1101/2022.03.21.485084>

864 53 Ou, J., Lan, W., Wu, X., Zhao, T., Duan, B., Yang, P., Ren, Y., Quan, L., Zhao, W., Seto,
865 D., Chodosh, J., Luo, Z., Wu, J. & Zhang, Q. Tracking SARS-CoV-2 Omicron diverse
866 spike gene mutations identifies multiple inter-variant recombination events. *Signal
867 Transduction and Targeted Therapy* **7**, 138 (2022). [https://doi.org/10.1038/s41392-022-00992-2](https://doi.org/10.1038/s41392-
868 022-00992-2)

869 54 Jeelani, R., Khan, S. N., Shaeib, F., Kohan-Ghadr, H. R., Aldhaheri, S. R., Najafi, T.,
870 Thakur, M., Morris, R. & Abu-Soud, H. M. Cyclophosphamide and acrolein induced
871 oxidative stress leading to deterioration of metaphase II mouse oocyte quality. *Free
872 Radic Biol Med* **110**, 11-18 (2017).
873 <https://doi.org/10.1016/j.freeradbiomed.2017.05.006>

874 55 Pimenta, G. F., Awata, W. M. C., Orlandin, G. G., Silva-Neto, J. A., Assis, V. O., da
875 Costa, R. M., Bruder-Nascimento, T., Tostes, R. C. & Tirapelli, C. R. Melatonin
876 prevents overproduction of reactive oxygen species and vascular dysfunction
877 induced by cyclophosphamide. *Life Sciences* **338**, 122361 (2024).
878 <https://doi.org/https://doi.org/10.1016/j.lfs.2023.122361>

879

880

881

882

883 **SUPPLEMENTARY TABLES**

884 **Table S1:** The number of samples per cohort, sample type and DPI that were
885 included in the sequencing analysis. Samples with less than 90% coverage and poor
886 or mediocre quality control results determined by Nextclade CLI, were excluded from
887 the analysis. *Multiple end point time-points due to humane end-point variation.

888

| Cohort | Sample type | DPI* | n |
|--------------------------------------------------------|-------------|--------|---|
| Cyclophosphamide and Molnupiravir | Swab | 1 | 4 |
| | | 3 | 4 |
| | | 5 | 3 |
| | Lung | 7 | 4 |
| | | Tissue | |
| | | | |
| | Nasal | 7 | 4 |
| | | Tissue | |
| | | | |
| Cyclophosphamide and Nirmatrelvir | Swab | 1 | 1 |
| | | 3 | 2 |
| | | 5 | 1 |
| | Lung | 4 | 1 |
| | | 7 | 2 |
| | | Tissue | |
| | Nasal | 4 | 1 |
| | | 7 | 2 |
| | | | |
| Cyclophosphamide only | Swab | 1 | 4 |
| | | 3 | 4 |
| | | 4 | 1 |
| | Lung | 5 | 2 |
| | | 4 | 2 |
| | | Tissue | |
| | Nasal | 6 | 2 |
| | | 4 | 1 |
| | | Tissue | |
| Cyclophosphamide, Nirmatrelvir and Molnupiravir | Swab | 6 | 2 |
| | | 1 | 1 |

| Cohort | Sample type | DPI* | n |
|---------------------|-------------|------|---|
| | Lung | 3 | 1 |
| | Tissue | 7 | 2 |
| | Nasal | 3 | 1 |
| | Tissue | 7 | 3 |
| Molnupiravir | Swab | 1 | 4 |
| | | 3 | 4 |
| | | 5 | 1 |
| | Lung | 7 | 3 |
| | Tissue | | |
| | Nasal | 7 | 1 |
| | Tissue | | |
| Vehicle | Swab | 1 | 4 |
| | | 3 | 4 |
| | | 5 | 4 |
| | Lung | 6 | 4 |
| | Tissue | | |
| | Nasal | 6 | 3 |
| | Tissue | | |

889

890

891

892

893

894 **Table S2:** Unique phenotypic changes in SARS-CoV-2 within the dataset. Input virus
895 amino acids and S: H665Y were excluded.

| Amino acid change | Occurrence in dataset | Tissue type | Cohorts |
|-------------------|-----------------------|-------------|-------------------------------------------------|
| S: D215H | 2 | Swab | Vehicle, Cyclophosphamide, Molnupiravir & |

| Amino acid change | Occurrence dataset | in | Tissue type | Cohorts |
|----------------------|-----------------------|----|----------------------|----------------------------------------------------------------------------------|
| | | | | nirmatrelvir |
| ORF1a: G2581S | 1 | | Swab | Cyclophosphamide & nirmatrelvir |
| ORF3a: P42L | 1 | | Swab | Cyclophosphamide & Molnupiravir |
| ORF3a: Q57H | 2 | | Nasal Tissue Swab | Cyclophosphamide, Molnupiravir & nirmatrelvir, Cyclophosphamide only |
| E: Y42H | 1 | | Swab | Cyclophosphamide & nirmatrelvir |
| ORF1a: G82D | 1 | | Lung Tissue | Cyclophosphamide, nirmatrelvir and Molnupiravir |
| S: V47I | | | | Cyclophosphamide, nirmatrelvir and Molnupiravir |
| ORF1a: T568I | 1 | | Nasal Tissue | Cyclophosphamide, |
| ORF1a: C2160Y | | | | nirmatrelvir and |
| ORF1b: F312L | | | | Molnupiravir |
| ORF1b: V251S | | | | |
| ORF8: F108L | | | | |
| S: A27T | | | | |
| ORF1a: F741L | 1 | | Nasal Tissue | Cyclophosphamide |
| ORF1a: A872T | | | | & nirmatrelvir |
| ORF7b: S5P | | | | |
| S: A890V | | | | |
| S: D985N | | | | |

| Amino acid change | Occurrence dataset | in | Tissue type | Cohorts |
|----------------------|-----------------------|----|--------------|--------------|
| ORF1a: F190L | 1 | | Nasal Tissue | Molnupiravir |
| ORF1a: G209S | | | | |
| ORF1a: V2130I | | | | |
| ORF1b: R1729H | | | | |
| ORF3a: M1I | | | | |
| ORF3a: G224S | | | | |
| S: S247R | | | | |
| S: V483I | | | | |

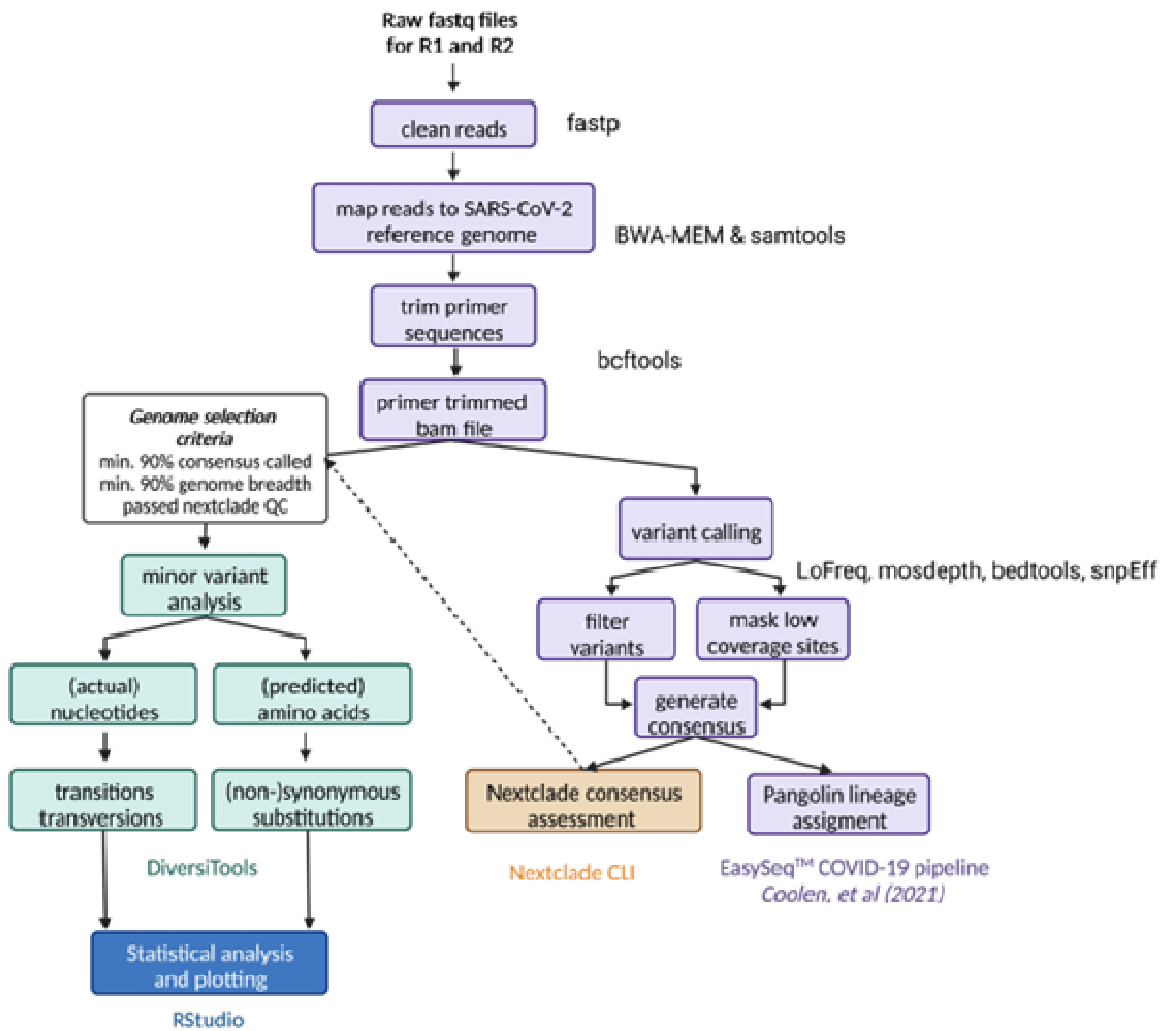
896

897

898

899 **Supplementary Figures**

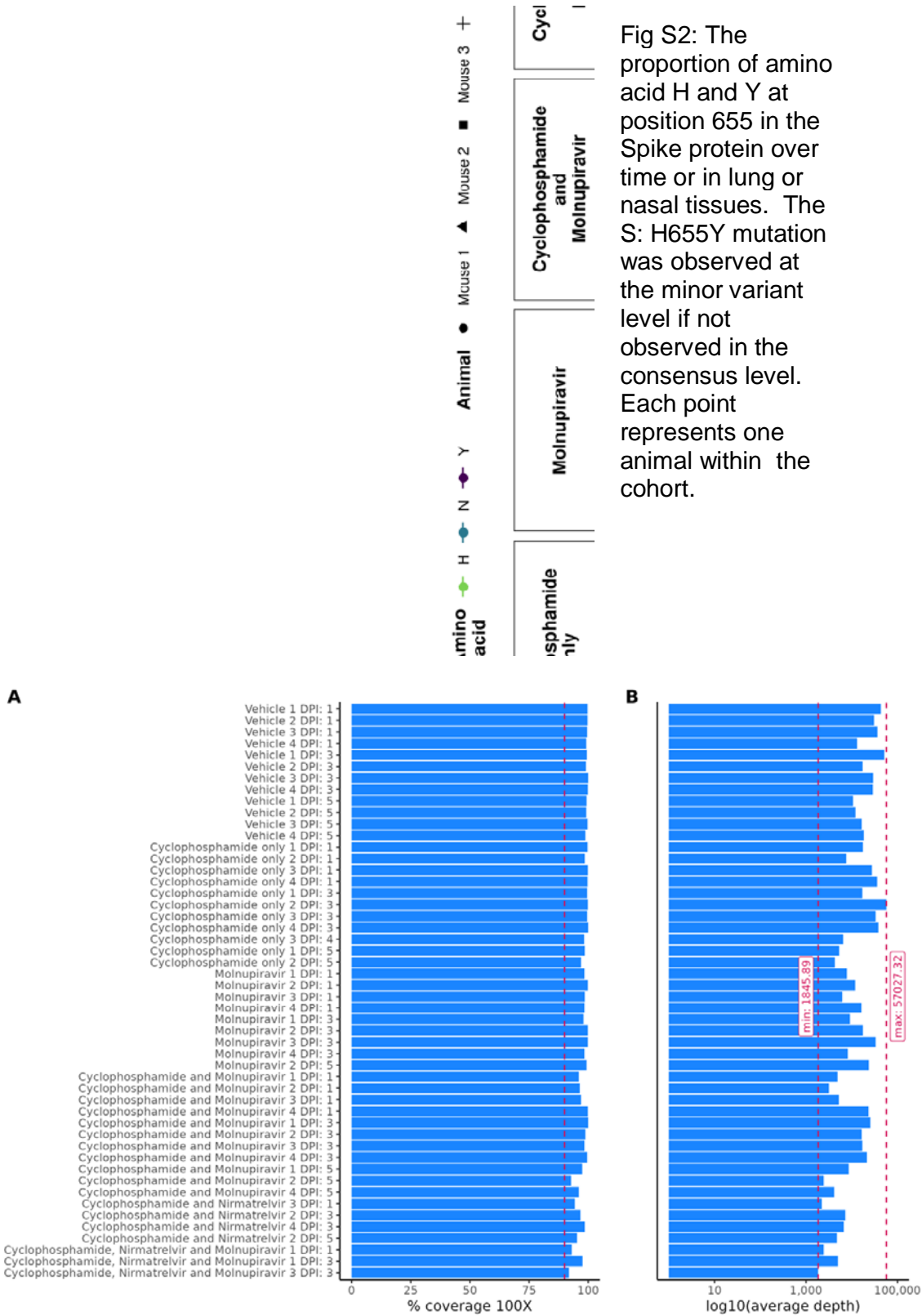
900 **Figure S1**



901

902 Fig S1: Bioinformatic workflow used for sequencing analysis.

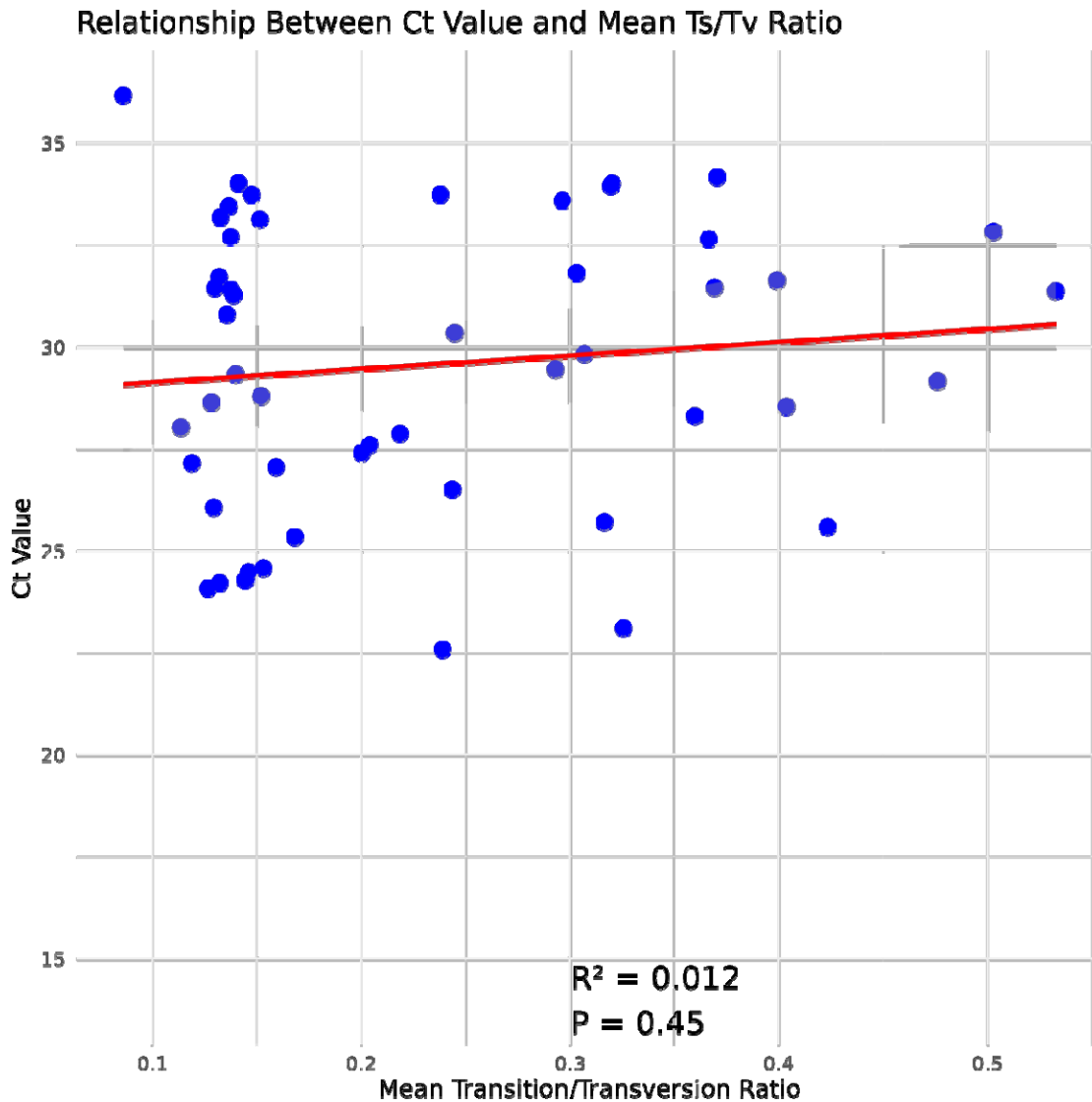
903
904



905
906
907
908

Fig S3: The coverage (A) and average depth (B) of the swabs used in the minor variant analysis.

909
910
911
912
913
914



915
916
917
918
919
920
921
922
923
924
925
926

Fig S4: The scatter plot shows the relationship between Ct values and the mean transition/transversion (Ts/Tv) ratios calculated with the DiversiTools output. Each blue dot represents a swab sample used in the minor variant analysis. The red line indicates the linear regression fit, with the shaded region showing the 95% confidence interval. Statistical analysis revealed no significant correlation between Ct values and Ts/Tv ratios ($R^2 = 0.012$, $p = 0.45$), supporting the conclusion that there is no association between the two variables.

927

928

929

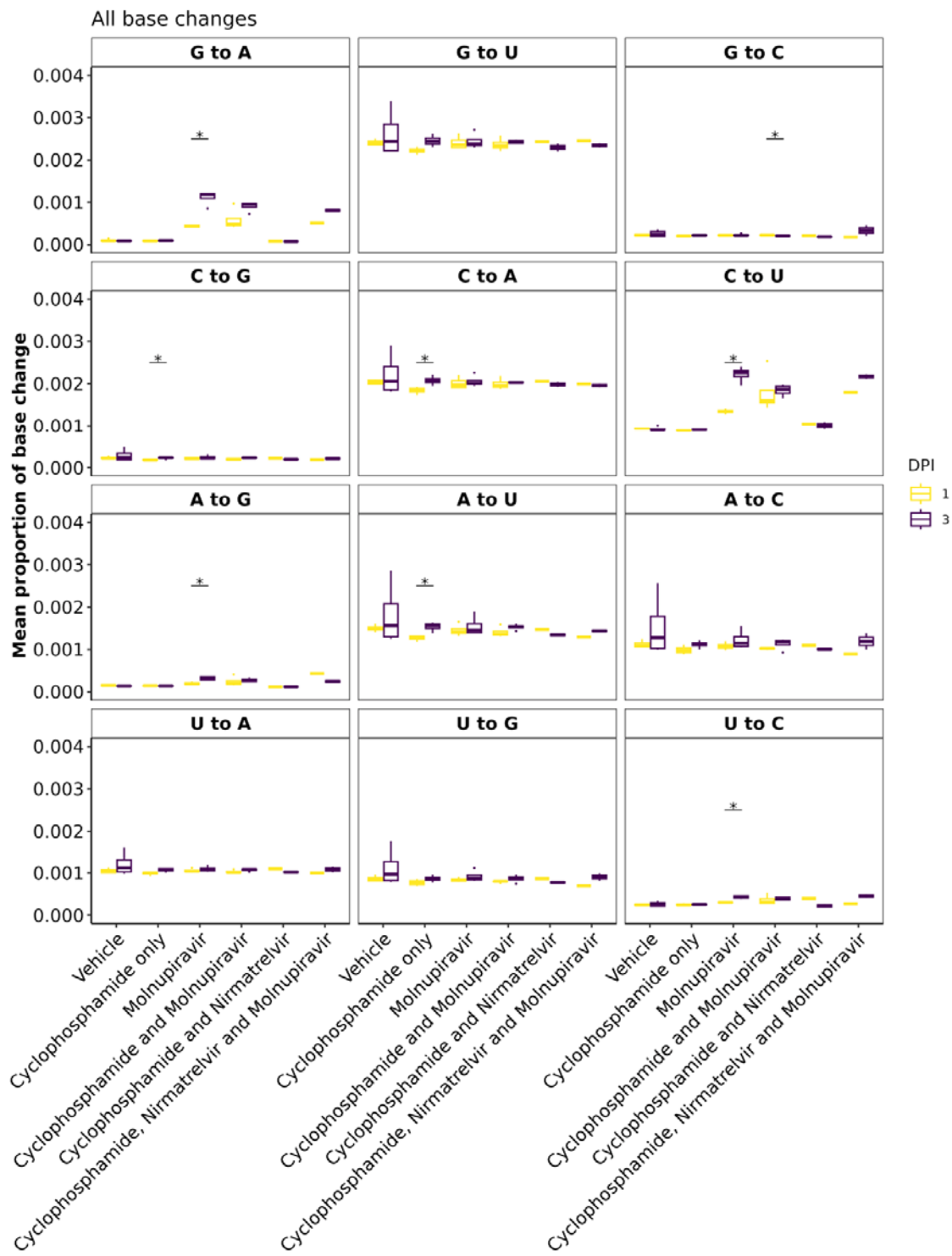
930

931

932

933

934



935

936

937

Fig S5: Minor variation for all base changes between day 1 and day 3 post infection.
 * represents a P value <0.05 (Mann Whitney U test).